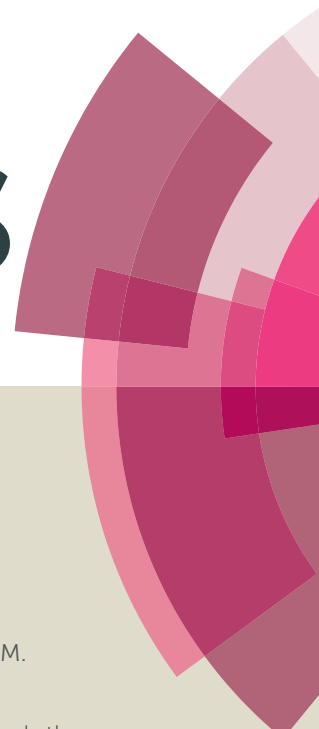


RSC Advances



This article can be cited before page numbers have been issued, to do this please use: A. Amoozegar, M. Haghghi and S. Aghamohammadi, *RSC Adv.*, 2016, DOI: 10.1039/C6RA02664H.



This is an *Accepted Manuscript*, which has been through the Royal Society of Chemistry peer review process and has been accepted for publication.

Accepted Manuscripts are published online shortly after acceptance, before technical editing, formatting and proof reading. Using this free service, authors can make their results available to the community, in citable form, before we publish the edited article. This *Accepted Manuscript* will be replaced by the edited, formatted and paginated article as soon as this is available.

You can find more information about *Accepted Manuscripts* in the [Information for Authors](#).

Please note that technical editing may introduce minor changes to the text and/or graphics, which may alter content. The journal's standard [Terms & Conditions](#) and the [Ethical guidelines](#) still apply. In no event shall the Royal Society of Chemistry be held responsible for any errors or omissions in this *Accepted Manuscript* or any consequences arising from the use of any information it contains.

Enhancement of Catalytic Properties and Lifetime of Nanostructured SAPO-34 by La Isomorphous Substitution and Alteration of Si/Al Ratio Used in Methanol to Light Olefins

Abolfazl Amoozegar^{1,2}, Mohammad Haghghi^{*1,2}, Sogand Aghamohammadi^{1,2}

1. Chemical Engineering Faculty, Sahand University of Technology, P.O.Box 51335-1996, Sahand New Town, Tabriz, Iran.

2. Reactor and Catalysis Research Center (RCRC), Sahand University of Technology, P.O.Box 51335-1996, Sahand New Town, Tabriz, Iran.

* Corresponding author:

Reactor and Catalysis Research Center, Sahand University of Technology, P.O. Box 51335-1996, Sahand New Town, Tabriz, Iran. Email: haghghi@sut.ac.ir, Tel: +98-41-33458096 & +98-41-33459152, Fax: +98-41-33444355, web: <http://rcrc.sut.ac.ir>

Abstract

Successful synthesis of nanostructured LaAPSO-34 catalysts with different Si/Al ratios being 0.1, 0.2, 0.3 and 0.4 were taken into account and used in methanol to light olefins. The catalysts were prepared via hydrothermal method and characterized by XRD, FESEM, PSD, EDX, TEM, BET, NH₃-TPD and FTIR techniques. The XRD results showed that the applied La ions preserve and complete the crystallite framework of the SAPO-34 resulted in higher crystallinity. It was found that the crystallinity of SAPO-34 increased upon Si incorporation up to Si/Al ratio of 0.3 and then followed by a decrease in intensity with further increase in silicon content. The FESEM micrographs for all the samples depict the cubic shaped typical crystals of CHA type zeotype structure. Si incorporation value was decreased by increasing the Si content in the initial gel. The stability test was conducted maintaining at constant operational conditions to distinguish the effect of time on stream. Consequently, coke formation has been delayed. The outstanding catalytic lifetime of the La modified catalyst with optimum Si content was reported to be 5500 min sustaining light olefins selectivity at higher values at diminished reaction temperature of 350°C.

Keywords: LaAPSO-34, Si/Al ratio, Methanol, Olefins, MTO.

1 Introduction

Ethylene and propylene are important petrochemicals feedstock, useful in a variety of processes for making plastics and other chemical compounds such as ethylene dichloride, ethylene oxide, propylene oxide, oxo-alcohol, polystyrene, acrylic acid and acrylonitrile. Demand for these key components is forecasted to increase over the next decade¹⁻³. The demand by 2015 is projected to grow up to 160 and 105 million tons for ethylene and propylene, respectively. At present, 97% of ethylene is produced from thermal steam cracking. Moreover, it produces propylene as a by-product which contributes to 66% of worldwide propylene production^{1,2}.

The preferred methanol conversion process is generally referred to methanol-to-olefins (MTO) process, where methanol is converted to primarily ethylene and/or propylene in the presence of a molecular sieve⁴⁻⁸. The oil crisis in 1970s caused a great interest in developing the methanol to hydrocarbons (MTH) technology as a vital alternative to the petroleum based route for the production of needed chemicals^{1,2,9}. Efforts were made to develop technologies for selective production of light olefins from methanol either on the medium-pore ZSM-5 zeolite^{10,11}, or later on small-pore SAPO-34 zeotype¹²⁻¹⁴. SAPO-34 molecular sieve with CHA structures, shows excellent performance in catalytic conversion of methanol to light olefins due to its moderate acidity and small 8-ring pore opening¹⁵⁻¹⁷. The small (about 4.7 Å) cages of SAPO-34 restrict the diffusion of heavy hydrocarbons, and this leads to high selectivity to the desired small light olefins¹⁸⁻²¹. The structure, acidity and catalytic performance of SAPO-34 catalyst directly depend on the number and distribution of Si in the framework²²⁻²⁴. The acidity of SAPO molecular sieves is generated by the hydroxyl groups, which originates from the protons for compensating the unbalanced electric charges due to Si incorporation into the neutral framework of AlPOs²⁵. Many researchers have studied the mechanism of Si incorporation into AlPOs framework and the Si substitution mechanism is

generally recognized in the crystallization process of SAPO molecular sieve. First, AlPOs structure is formed, then Si atoms is incorporated into the AlPOs framework by isomorphous substitution. It is a general rule that the linkage of the type Si-O-P is avoided. It is recognized that there exist two kinds of Si substitution mechanisms in the crystallization of SAPO molecular sieves. One is the substitution of P by Si (denoted as SM2), which would form Si(4Al) entities. The other is the double substitution of adjacent P and Al by two Si atoms (denoted as SM3), which gives rise to Si(nAl) ($n = 3-0$) structures and stronger Brønsted acid sites²⁶. Hence, the catalytic properties of the SAPO should depend at least to some extent on the relative occurrence of both substitution mechanisms. Therefore, the silica content is the controlling variable which determines the relative ratio of acid sites of different strength. It was proposed that Si incorporation by the first mechanism formed Si(4Al) structures when the SiO₂/Al₂O₃ molar ratio was low in starting gel. While for starting gel with increasing SiO₂/Al₂O₃ molar ratio, Si(3Al), Si(2Al), Si(1Al) and Si(0Al) structures were formed simultaneously by the second mechanism²⁶⁻²⁸.

A main problem associated with the applied SAPO-34 molecular sieve is the rapid deactivation due to coke deposition during MTO reaction, leading to a serious decrease in activity and selectivity of SAPO-34^{29,30}. For this reason, increasing the ability of the catalyst to resist coke formation is a key challenge that is urgently required for the practical MTO application^{31,32}. Metal doping as a convenient way to control or alter the catalytic behaviour was extensively investigated for MTO reaction with the goal of modifying the acidity of the SAPO-34 and adjusting the strength of T-O bond in the TO₄ tetrahedral unit of the SAPO-34 framework. A method of enhancing the catalyst lifetime and simultaneously avoiding the formation of methane during the MTO process is metal introduction into the SAPO-34 framework³³⁻³⁵. However, the previously published articles mainly paid attention to the transition metals but, effect of rare earth metal doping on the lifetime of the SAPO-34

catalyst have not been taken into account in detail especially with the isomorphous substitution method. It has been reported that La-doped SAPO-34 catalysts with solid state ion exchange method resulted in higher selectivity of light olefins and reduced amount of methane compared to the ones prepared without metal addition³⁶. In the present work, lanthanum was chosen to be used for SAPO-34 modification by the isomorphous substitution method.

In this paper, a series of SAPO-34 molecular sieves with La-incorporation were synthesized with different Si/Al ratios. In addition, the catalyst obtained by optimum Si content was synthesized without metal addition to explore the metal influence. The physicochemical properties of the molecular sieves were characterized using XRD, FESEM, PSD, EDX, BET, NH₃-TPD and FTIR techniques. The characterization of materials followed by the testing of samples for catalytic performance qualities such as reactivity (activity and selectivity) and stability (lifetime) allows us to gain deeper insights into the relationship between structure and catalytic properties.

2 Materials and Methods

2.1 Materials

The reactants used for preparation of LaAPSO-34 samples were aluminium tri- isopropylate (Aldrich, 98+ %), fumed silica (Aldrich, 99.9%), phosphoric acid (Merck, 85% aqueous solution), lanthanum nitrate hexahydrate (Merck, 99%) as the sources of Al, Si, P and La, respectively. TEAOH (Aldrich, 20%) was used as the organic template.

2.2 Preparation and Procedures

The details of LaAPSO-34 synthesis with different Si contents are shown in Figure 1. The synthesized catalysts with Si/Al ratio of 0.1, 0.2, 0.3 and 0.4 were denoted as LaAPSO-34

(0.1), LaAPSO-34 (0.2), LaAPSO-34 (0.3) and LaAPSO-34 (0.4), respectively. To elucidate the effect of metal addition, the LaAPSO-34 (0.3) sample was synthesized without metal introduction and named SAPO-34 (0.3). The molar composition of synthesis solution was 2TEAOH: 1Al₂O₃: xSiO₂: 0.05La₂O₃: 1P₂O₅: 70H₂O. The parameter x, took the values of 0.2, 0.4, 0.6 and 0.8. In detail, weighted aluminium tri- isopropylate was dissolved in TEAOH for 90 min. Fumed silica and lanthanum nitrate were added to the solution in turn. Finally, phosphoric acid was gradually added and it was continually stirred for 24 h. The resulting gel was transferred into a stainless autoclave and heated at 200°C for 72 h. The resulting solids were collected by centrifugation, washed with water and dried overnight at 110°C. Finally, the catalyst sample was calcined at 550°C for 12 h to remove organic template and trapped water within the micro pores of the as-synthesized solid.

(Figure 1)

2.3 Characterization Techniques

XRD patterns were recorded on a Bruker D8 Advance diffractometer with Cu K α radiation (1.54178 Å) to identify crystal phases. The phase identification was made by comparison to the Joint Committee on Powder Diffraction Standards (JCPDSs). The average crystal size was calculated using the half-width at half-height of most intense peaks of diffraction pattern and well-known Debye-Scherrer equation. The morphology of the samples was observed by the Field Emission Scanning Electron Microscopy (FESEM) on a HITACHI S-4160 (Japan). For reporting particle size distribution we used ImageJ software. Using this image analyser, we find particles size in selected FESEM micrograph which shown in the figure. Some statics have been performed to find the minimum, maximum and average particle size of the samples by this software. The number of particles have been taken into account was 60. The

FESEM was equipped with an Energy Dispersive X-ray (EDX) analyzer to carry out dot maps for dispersion analysis. Transmission electron microscopy (TEM) was carried out on a Philips CM-200. Samples for TEM measurements were ultrasonically dispersed in ethanol. The specific surface area of the sample was determined by N₂ adsorption-desorption method at -196°C on a surface area analyzer (Quantachrome ChemBET-3000). FTIR spectra of the samples were recorded on a UNICAM 4600 FTIR spectroscopy using KBr pellet. Catalysts acidity was measured by ammonia temperature programmed desorption using BELCAT analyser with a TCD detector. Before analysis, 0.1g of calcined sample was preheated at 550°C for 60 min under a 50 cm³/min helium gas flow. Ammonia adsorption was made from a mixture of 5% (molar basis) of ammonia in helium under total flow rate of 50 cm³/min at 100°C. After adsorption of ammonia, the samples were kept under a helium gas flow at 100°C to remove physically adsorbed gases. Finally, the helium flow (50 cm³/min) was passed through the sample with increasing temperature up to 800°C at a rate of 10°C/m.

2.4 Experimental Setup for Catalytic Performance Test

The experimental setup used in this study is presented in Figure 2. Catalytic reaction studies were performed in a fixed bed U-shaped Pyrex reactor under atmospheric pressure. The certain amount of catalyst (0.4 g) was loaded and prior to the reaction preheated using 70 ml/min argon at 500°C for 60 min to remove the adsorbed water and then cooled to reaction temperature. The liquid mixture of methanol and water with molar ratio of 30:70 was fed to the reactor by passing argon flow through the saturator. All reactions were carried out at constant gas hourly space velocity (GHSV= 4200 cm³/g.h). The saturator temperature was kept at 8-9°C by using an ice bath. The rate of carrier gas is adjustment with a mass flow controller (MFC). The products were analyzed on gas chromatograph (GC Chrom, Teif Gostar Faraz, Iran) with flame ionization detector (FID) using Plot-U (Agilent) column by

programming the oven temperature between 40 and 180°C. Argon was used as a carrier gas and hydrogen was used in FID. Typical material balance was carried out for some of the experiments and it was found that the value is within the error limit ($\pm 3\%$).

(Figure 2)

3 Results and Discussions

3.1 Physicochemical Characterizations

3.1.1 XRD Analysis

XRD patterns of the catalysts synthesized via hydrothermal method are shown in Figure 3. All the five samples possess SAPO-34 rhombohedral structure with the strongest XRD diffraction at $2\theta = 9.5$ (JCPDS 01-087-1527)^{3, 26, 37, 38}. But, some special diffractions at $2\theta = 19.8, 21.0$ and 22.4 corresponding to SAPO-5 phase (JCPDS 00-049-0659)^{39, 40} can be found for the sample with lower Si content (Si/Al = 0.1). The SAPO-5 phase content is negligible for LaAPSO-34 (0.1). It will be demonstrated that the typical diffractive peaks and crystallites of SAPO-5 cannot be easily monitored by the XRD and FESEM analyses. By further increase of Si content, the minor peaks of SAPO-5 were disappeared for the LaAPSO-34 (0.2) sample. Furthermore, no assignable peak to metal oxide (La_2O_3) was observed for the metal containing samples. The effect of Si/Al ratio was estimated from the XRD spectra and it was found that the crystallinity of SAPO-34 increased upon Si incorporation up to LaAPSO-34 (0.3) and then followed by a decrease in intensity with further increase in the silicon content. To elucidate the effect of metal addition, the LaAPSO-34 (0.3) sample was synthesized without metal introduction. The XRD results show that the applied La ions preserve and complete the crystallite framework of SAPO-34 resulted in higher crystallinity.

Thermal stability of the samples can be confirmed by the observation of all characteristic peaks of SAPO-34.

Relative crystallinity and crystallite size of the samples were calculated based on the peak intensity at $2\theta = 9.5$ and Scherrer equation, respectively (Figure 4). The obtained crystallite size was in a range of 23 to 43 nm, confirming the nanostructure framework of the synthesized samples. It should be noticed that nanostructure and well-defined framework of the catalysts can resultantly make them highly desired material for catalytic processes. Relative crystallinity was calculated to be 49, 54.9, 87.4, 100 and 43% for LaAPSO-34 (0.1), LaAPSO-34 (0.2), SAPO-34 (0.3), LaAPSO-34 (0.3) and LaAPSO-34 (0.4), respectively confirming the observed intensity variation of diffractive peaks. Most of the crystallinity reduction occurred when the Si content increased from 0.3 to 0.4 for which the obtained relative crystallinity is lower than that of the sample prepared with the lowest Si. It can be explained in a way that the further increase of Si ions in the initial gel cannot incorporate into the crystallite framework, leading to recrystallization and/or formation of amorphous phase. The lattice parameters of SAPO-34 and LaAPSO-34 samples are shown in **Error! Reference source not found.** As seen, by introducing La into structure of SAPO-34, lattice parameters changed and volume increased. It confirmed isomorphously substitution of La into SAPO-34 in SAPO-34 sample. As, due to the low lanthanum oxide on the surface of crystals and well dispersion of it, related peaks to lanthanum oxide were not observed in the patterns of samples with La loading.

(Figure 3)

(Figure 4)

(Error! Reference source not found.)

3.1.2 FESEM Analysis

Figure 5 shows the FESEM images of the synthesized catalysts to investigate the effect of increasing Si/Al ratio on morphology. The scanning electron micrographs for all the samples depict the cubic shaped typical crystals of CHA type zeotype structure reported in literature⁴¹⁻⁴³. It is obvious that variation of particle sizes and morphology arises from various Si loadings into the SAPO-34 structure. XRD pattern of the LaAPSO-34 (0.1) sample confirmed the presence of SAPO-5 structure which is not observed by the corresponding typical hexagonal like particles. It can afford additional support for the minor formation of the SAPO-5 impurity phase evidenced by the XRD analysis. As indicated, metal addition resulted in smoother and a little bit larger particles. Thus, it can be implied that the presence of La heteroatoms in the precursors solution did not result in any distribution of the SAPO-34 framework and also enhance the relative crystallinity.

At lower Si content, crystallite framework of the SAPO-34 structure did not formed completely and some regions of amorphous particles can be easily detected from the FESEM images. By gradual increase of Si/Al ratio, much more smoother and cubic like particles appeared diminishing the roughness of the particles surface. However, the increase of Si/Al ratio from 0.3 to 0.4 leads to the formation of some non-cubic particles confirming the crystallinity loss due to the recrystallization process and/or amorphous phase formation. Completing the SAPO-34 structure by Si increasing happens with the different Si substitution mechanisms (SM2 and SM3). At lower Si loadings, the SM2 is dominant but the SM3 also becomes dominant at higher Si contents. As discussed, the relative crystallite phase decomposition can be the disadvantageous side effect of the further Si introduction. It can be explored in terms of catalytic performance during the MTO reaction.

(Figure 5)

3.1.3 PSD Analysis

Particle size distribution (PSD) of the samples has been calculated using ImageJ software⁴⁴ and illustrated in Figure 6. The average particle size was calculated to be 0.7 and 1.3 μm for the SAPO-34 (0.3) and LaAPSO-34 (0.3) samples, respectively. It seems that the samples with higher crystallinity appeared with much more smoother and larger particles in FESEM micrographs that it confirms the accordance of the results of XRD and FESEM analyses. Particle size and its distribution have great influences on the performance of SAPO-34 catalysts applied for the MTO reaction.

(Figure 6)

3.1.4 EDX Analysis

Figure 7 shows the EDX dot-mapping of Al, Si, P and La for the synthesized catalysts. Presence of all used elements in the corresponding EDX spectrums and results of former analyses proves the successful hydrothermal synthesis. The determination of metal amount was carried out with EDX analysis and compared with the initial gel composition as depicted in Figure 8. The obtained materials and the initial gel compositions are relatively close to each other. The Al and P elements of LaAPSO-34 samples were the most scattered elements which is simply observable by the EDX spectra and their dot-mappings. Si dot-mapping exhibited with the highest dispersion for the LaAPSO-34 (0.3) sample compared to the Si distribution of the other samples. Another detectable difference may be attributed to the La heteroatoms distribution on the surface which is responsible for enhancing the stability of SAPO-34. It has the same trend as mentioned for the Si dispersion on the surface of the catalysts and higher dispersion of the La was obtained for LaAPSO-34 (0.3). Thus, applying Si/Al ratio of 0.3 resulted in higher dispersion of Si and La. It is better to make a comparison

between the Si content of the initial gel and the synthesized samples to discuss the Si incorporation. The $\text{Si}/(\text{Al}+\text{P}+\text{Si}+\text{La})$ value of all the starting gels and the values for the prepared solid products are quite different, indicating that different amount of Si was incorporated in to the SAPO-34 framework by applying different Si/Al ratio. Si incorporation was defined as the ratio of the $[\text{Si}/(\text{Al}+\text{P}+\text{Si}+\text{La})_{\text{solid}}]/[\text{Si}/(\text{Al}+\text{P}+\text{Si}+\text{La})_{\text{gel}}]$. It is calculated to be 2.33, 1.25, 1.11 and 0.97 for the LaAPSO-34 (0.1), LaAPSO-34 (0.2), LaAPSO-34 (0.3) and LaAPSO-34 (0.4), respectively. Si incorporation value was decreased by increasing the Si content in the initial gel. It is indicative of the incapability of the crystallite framework to incorporate higher amounts of Si. Si content and its distribution in the SAPO-34 framework might have great impact on the catalytic behaviour of the catalysts.

(Figure 7)

(Figure 8)

3.1.5 TEM Analysis

TEM images of the LaAPSO-34 (0.3) catalyst synthesized were illustrated in Figure 9. The production of some nanometer scale particles alongside bigger ones can be clearly observed from the corresponding TEM images. Nanocatalysis research can be explained as the preparation of heterogeneous catalysts in the nanometer length scale. They are very promising and it can be expected that use of them can decrease the energy usage in the chemical processes results in a greener chemical industry.

(Figure 9)

3.1.6 BET Analysis

The total specific surface area of the synthesized samples was measured and reported in Figure 10. It is obvious that the use of La heteroatom caused the increase of specific surface area comparing to the one prepared without metal. It can be explained by the further growth of the SAPO-34 crystallite framework in the presence of metal ions in the initial gel. The increase of Si/Al ratio from 0.1 to 0.3 resulted in an increase of specific surface area from 425 to 528 m²/g and then followed by a decrease to 443 m²/g for the LaAPSO-34 (0.4). The observed trend for the variation of surface area was seen for the relative crystallinity. It can be implied that the increase of Si/Al ratio up to 0.3 leads to the structure completeness. Consequently, enhancement of crystallinity and particles smoothness cause the increase of specific surface area. The highest specific surface area was achieved for the catalyst with the highest crystallinity so results of BET analysis are in well agreement with XRD analysis. Active sites availability for the MTO reaction has a relationship with the specific surface area of the catalysts. It is expected that the LaAPSO-34 (0.3) with the highest specific surface area and much more availability of active sites is going to have excellent catalytic performance.

(Figure 10)

3.1.7 FTIR Analysis

Figure 11 illustrates the FTIR spectra of the calcined catalysts that synthesized with different Si contents. Characteristic peaks of SAPO-34 were identified at wave numbers 480, 635, 715 and 1110 cm⁻¹ for all the samples^{45,46}. The peaks at 480, 530 and 570 cm⁻¹ are assignable to the bending vibrations of SiO₄, AlO₄ and PO₄, respectively^{26,47}. Furthermore, peak located at 635 cm⁻¹ can be attributed to the T-O bending in D-6 rings^{37,45}. Symmetric and asymmetric vibration of the O-P-O can be observed at wavenumber of 715 and 1110 cm⁻¹, respectively⁴⁸.

Major peaks positions did not change with La addition which is in accordance with the corresponding XRD analysis. Moreover, no displacement of the characteristic peaks of SAPO-34 was monitored by increasing the Si/Al ratio. Peaks at wavenumber of 2350 and 2450 cm^{-1} can be attributed to the physically adsorption of CO and CO_2 from surrounding^{38, 49, 50}. The peak at wavenumber of 3450 cm^{-1} can be attributed to bridging hydroxyl groups⁵¹⁻⁵³. Si-OH-Al bridges position and intensity of them in the IR spectra can provide information to judge about the products acidity^{17, 54, 55}. The peak at wavenumber of 1650 cm^{-1} is assigned to physical adsorption of the H_2O molecules on the samples surface^{52, 56, 57}.

(Figure 11)

3.1.8 TPD- NH_3 Analysis

The TPD profiles of ammonia desorption on LaAPSO-34 (0.2), SAPO-34 (0.3) and LaAPSO-34(0.3) catalysts are presented in Figure 12 to determine the concentration and strength of acid sites. Two desorption peaks are clearly observed for all of the samples. The stronger acid sites exhibits with a higher desorption temperature resulting in higher values of temperature maxima in TPD patterns. Furthermore, the area underlying the curves indicates the amount of ammonia indicative of acid sites concentration. Ammonia desorption peaks approximately centered at 176-179°C for weak acid sites and 392-423°C for strong acid sites. The first peak attributes to the weak acid sites representing the defect structural OH groups (including Si-OH, P-OH and Al-OH). The second desorption peak belongs to the strong acid sites, related to Si-OH-Al groups (Brønsted acidic sites). As indicated, weak acid sites density was decreased by the increase of Si/Al ratio from 0.2 to 0.3. But its strength did not modify considering the peaks maxima for the LaAPSO-34 (0.2) and LaAPSO-34 (0.3) catalysts. The same phenomenon occurred for high temperature peaks by the increase of Si/Al ratio. The

SAPO-34 (0.3) sample showed higher desorption temperatures for both weak and strong acid sites than the LaAPSO-34 (0.3) catalyst. Furthermore, it indicates that metal introduction resulted in decrease of strong acid sites strength compared to the SAPO-34 by the observation of high temperature peak shift to lower temperatures. It has been proved that weak acid sites do not have any strong effect in MTO reaction and these sites can only produce DME and water from dehydration of methanol. On the other hand, strong acid sites (located in zone 2) have a critical role in the formation of light olefins from DME. However, stronger acid sites would also promote coke formation reactions and lead to the fast catalyst deactivation. As seen, the concentration of both weak and strong acid sites for the LaAPSO-34 (0.3) catalyst is lower than that of SAPO-34 catalyst. NH_3 -TPD results indicate that La incorporation led to the decrease of acid sites concentration and strength. The high concentration of acid sites has positive effect on olefins selectivity and increasing lifetime. On the other hand, increasing strength of acid sites has negative effect on MTO performance especially in viewpoint of lifetime.

(Figure 12)

3.2 Catalytic Performance Study toward Methanol to Light Olefins Conversion

3.2.1 Effect of Temperature on Methanol Conversion and Products Selectivity

Methanol conversion and products distribution at temperatures ranging from 300 to 500°C over LaAPSO-34 (0.1) catalyst was studied as shown in Figure 13. All the reactions were carried out at constant feed composition and GHSV. Methanol conversion increased and reached a maximum value of 100% at 400°C. The observed trend has been reported for the other samples too. Ethylene selectivity increased up to 400°C and then decreased. Moreover, propylene and higher hydrocarbons selectivity followed a continuous decreasing trend by the

increasing temperature. Methane is considered an undesired by-product of the MTO reaction. Methane formation has been enhanced at higher temperatures. The highest value of the methane selectivity was obtained at 500°C to be 74%. Thus, lower temperatures are favour to achieve the highest selectivity of the light olefins. Propylene and higher hydrocarbons conversion to ethylene occurs dominantly resulting in higher ethylene selectivity. But, methane formation side reactions play a major role at higher temperatures and consequently, ethylene selectivity starts decreasing. As a result, operational temperature can be a key parameter to achieve the desired selectivity of the light olefins.

(Figure 13)

3.2.2 Effect of La Addition on Methanol Conversion and Products Selectivity

Methanol conversion at various temperatures for SAPO-34 (0.3) and LaAPSO-34 (0.3) catalysts is depicted in Figure 14. At higher temperatures, above 400°C, methanol conversion was complete for both of the catalysts. However, the SAPO-34 catalyst with metal introduced gains higher values of methanol conversion even at low temperatures of 300 and 350°C. It was proved that the La addition during the synthesis has a positive effect on crystallinity and specific surface area. Therefore, active sites availability towards feed molecules would be enhanced.

Figure 15 illustrates the effect of La addition on olefins selectivity, C₂H₄ (a) and C₃H₆ (b). At 400°C, ethylene selectivity reaches a maximum of 70 and 63 % for the LaAPSO-34 (0.3) and SAPO-34 (0.3) samples, respectively. Afterward, it followed a decreasing trend. In addition, propylene selectivity reached the maximum at 300°C for both of the catalysts. For all the examined temperatures, light olefins selectivity for the metal containing sample was

enhanced compared to the sample synthesized without metal. It is due to the increased crystallinity and specific surface area of the La modified SAPO-34.

Figure 16 shows the effect of the La addition on methane selectivity for the SAPO-34 (0.3) and LaAPSO-34 (0.3) catalysts. Methane formation was limited for the catalyst synthesized with metal. For instance, there was no methane at 300 and 350°C for the LaAPSO-34 (0.3) catalyst. The best operating temperature with respect to light olefins selectivity was 350 and 400°C for the LaAPSO-34 (0.3) and SAPO-34 (0.3) samples, respectively. In the other words, by incorporation of La into the structure of SAPO-34, optimum temperature for the process was reduced. This point is significant from an economic point of view. However, the stability test was carried out at 350°C to make a good comparison.

(Figure 14)

(Figure 15)

(Figure 16)

3.2.3 Effect of Si/Al Ratio on Methanol Conversion and Products Selectivity

The time dependence selectivity of the major products and methanol conversion over the synthesized samples was shown in Figure 17. The stability test has been carried out for all the five samples at 350°C and constant GHSV. Long term behaviour of the catalysts can be investigated in terms of Si/Al ratio and also La heteroatom introduction. As indicated, methanol conversion and light olefins selectivity reached at about 85 and 60%, respectively after about 2400 min for the SAPO-34 (0.3). Moreover, LaAPSO-34 (0.3) catalyst exhibited superior activity for which methanol conversion and light olefins selectivity reached at about 90 and 60%, respectively at TOS = 5500 min. The time of reaction sustaining light olefins selectivity at about 60% was selected as a criterion to evaluate the long term behaviour of the

catalysts. Stability test results of the LaAPSO-34 (0.3) and SAPO-34 (0.3) samples can provide excellent information about the effect of La addition on the catalytic performance of SAPO-34. Higher specific surface area, proper acid sites density and proper crystallinity of the LaAPSO-34 (0.3) can provide much more active sites for the MTO reaction. Thus, it takes longer time for the LaAPSO-34 (0.3) to deactivate at constant operational conditions. Moreover, La incorporation into the crystalline framework would diminish the effect of side reactions by probably adjustment of the active sites density and their strength. Consequently, coke formation would be delayed. Appearance of DME in the products can illustrate beginning of catalyst deactivation. With catalyst deactivation by coke deposition, the strong acid sites poison with coke. But, DME can be produced on weak acid sites that these active sites are not capable of converting DME to light olefins. As seen, for the SAPO-34 (0.3) sample DME appeared after 1350 min of reaction and then increased. For LaAPSO-34 (0.3), DME produced at later times (2200 min) and also increased with a lower rate for which milder Brønsted acid sites can be the main reason.

Conversion elimination is not so much and can be neglected. It can be attributed to the conversion of methanol to dimethyl ether (DME) on weakened acid centres by the further coke deposition. DME can be easily obtained from methanol dehydration by using catalysts with lower acidity. The reaction time at which light olefins selectivity reaches at about 60% was reported to be 2400, 2700, 5500 and 3300 min for the LaAPSO-34 (0.1), LaAPSO-34 (0.2), LaAPSO-34 (0.3) and LaAPSO-34 (0.4), respectively. The higher specific surface area and crystallinity evidenced by BET and XRD techniques can be the reasons for the best catalytic performance of the LaAPSO-34 (0.3). Furthermore, it seems that catalyst lifetime was prolonged by increasing Si/Al ratio from 0.1 to 0.3. But, further increase of Si content had an adverse effect on the stability of the catalyst. It can be a meaningful relationship between the physiochemical characteristics of the catalyst and their lifetime during the

reaction. Increase of Si/Al ratio up to 0.3 resulted in specific surface area and crystallinity enhancement. Consequently, stable MTO reaction was expected for the LaAPSO-34 (0.3). As mentioned before, all the stability tests were conducted at 350°C. Therefore, negligible methane formation can be due to the applied low temperature. Another noticeable point may be attributed to the variation of ethylene and propylene selectivity toward the time progress. Ethylene selectivity showed an increasing trend at earlier times of reaction and then decreased. However, propylene started decreasing from the onset of reaction to the end of analysis. Channels and pore mouths of the applied molecular sieve can be partially blocked by the higher hydrocarbon molecules known as hydrocarbon pool intermediates like methylnaphthalenes, phenanthrene and pyrene. Consequently, propylene diffusivity would be decreased and resultantly its cracking to ethylene could be happened. However, due to further coke deposition and complete blockage of some channels, selectivity of both C₂H₄ and C₃H₆ decreased at longer times.

(Figure 17)

4 Conclusions

The higher specific surface area and crystallinity evidenced by BET and XRD techniques can be the reasons for the best catalytic performance of LaAPSO-34 (0.3). It seems that catalyst lifetime was prolonged by increasing Si/Al ratio from 0.1 to 0.3. But, further increase of Si content had an adverse effect on the stability of the catalyst. The reaction time at which light olefins selectivity reaches at about 60% was reported to be 2400, 2700, 5500 and 3300 min for the LaAPSO-34 (0.1), LaAPSO-34 (0.2), LaAPSO-34 (0.3) and LaAPSO-34 (0.4) samples, respectively. The excellent stability of the synthesized catalyst with Si/Al ratio of 0.3 and simultaneous metal introduction can be known as a novel one for the MTO reaction

which gains higher values of desired products at complete methanol conversion and lower temperature of 350°C.

Acknowledgements

The authors gratefully acknowledge Sahand University of Technology for the financial support of the research as well as Iran Nanotechnology Initiative Council for complementary financial supports.

References

1. Q. Ji, *Computers & Industrial Engineering*, 2012, **63**, 615-625.
2. H. Schmidbauer and A. Rösch, *Energy Economics*, 2012, **34**, 1656-1663.
3. F. M. Shalmani, R. Halladj and S. Askari, *Powder Technology*, 2012, **221**, 395-402.
4. P. Wang, A. Lv, J. Hu, J. a. Xu and G. Lu, *Microporous and Mesoporous Materials*, 2012, **152**, 178-184.
5. S. Askari, R. Halladj and M. Sohrabi, *Microporous and Mesoporous Materials*, 2012, **163**, 334-342.
6. Y.-J. Lee, S.-C. Baek and K.-W. Jun, *Applied Catalysis A: General*, 2007, **329**, 130-136.
7. D. R. Dubois, D. L. Obrzut, J. Liu, J. Thundimadathil, P. M. Adekkanattu, J. A. Guin, A. Punnoose and M. S. Seehra, *Fuel Processing Technology*, 2003, **83**, 203-218.
8. L. Xu, Z. Liu, A. Du, Y. Wei and Z. Sun, in *Studies in Surface Science and Catalysis*, eds. B. Xinhe and X. Yide, Elsevier, Editon edn., 2004, vol. Volume 147, pp. 445-450.
9. R. Wei, C. Li, C. Yang and H. Shan, *Journal of Natural Gas Chemistry*, 2011, **20**, 261-265.
10. M. Firoozi, M. Baghalha and M. Asadi, *Catalysis Communications*, 2009, **10**, 1582-1585.
11. M. Bejblova, N. Zilkova and J. Cejka, *Research on Chemical Intermediates*, 2008, **34**, 439-454.
12. T. Alvaro-Munoz, C. Marquez-Alvarez and E. Sastre, *Catalysis Today*, 2013, **213**, 219-225.
13. B. Vora, J. Q. Chen, A. Bozzano, B. Glover and P. Barger, *Catalysis Today*, 2009, **141**, 77-83.
14. P. Sadeghpour and M. Haghghi, *Journal of Advanced Materials and Processing*, 2014, **2**, 49-66.
15. S. Wilson and P. Barger, *Microporous and Mesoporous Materials*, 1999, **29**, 117-126.
16. W. Shen, X. Li, Y. Wei, P. Tian, F. Deng, X. Han and X. Bao, *Microporous and Mesoporous Materials*, 2012, **158**, 19-25.
17. S. Aghamohammadi, M. Haghghi and M. Charchand, *Materials Research Bulletin*, 2014, **50**, 462-475.
18. D. Chen, K. Moljord, T. Fuglerud and A. Holmen, *Microporous and Mesoporous Materials*, 1999, **29**, 191-203.

19. G. Liu, P. Tian and Z. Liu, *Chinese Journal of Catalysis*, 2012, **33**, 174-182.
20. P. Wang, D. Yang, J. Hu, J. a. Xu and G. Lu, *Catalysis Today*, 2013, **212**, 62.e61-62.e68.
21. M. Inoue, P. Dhupatemiya, S. Phatanasri and I. Tomoyuki, *Microporous and Mesoporous Materials*, 1999, **28**, 19-24.
22. Q. Wang, L. Wang, H. Wang, Z. Li, X. Zhang, S. Zhang and K. Zhou, *Frontiers of Chemical Engineering in China*, 2011, **5**, 79-88.
23. T. Wang, X. Lu and Y. Yan, *Microporous and Mesoporous Materials*, 2013, **168**, 155-163.
24. S. Ashtekar, S. V. V. Chilukuri and D. K. Chakrabarty, *The Journal of Physical Chemistry*, 1994, **98**, 4878-4883.
25. P. Sadeghpour and M. Haghighi, *Particuology*, 2015, **19**, 69-81.
26. J. Tan, Z. Liu, X. Bao, X. Liu, X. Han, C. He and R. Zhai, *Microporous and Mesoporous Materials*, 2002, **53**, 97-108.
27. L. Xu, A. Du, Y. Wei, Y. Wang, Z. Yu, Y. He, X. Zhang and Z. Liu, *Microporous and Mesoporous Materials*, 2008, **115**, 332-337.
28. A. Izadbakhsh, F. Farhadi, F. Khorasheh, S. Sahebdehfar, M. Asadi and Y. Z. Feng, *Applied Catalysis A: General*, 2009, **364**, 48-56.
29. J. Liang, H. Li, S. Zhao, W. Guo, R. Wang and M. Ying, *Applied Catalysis*, 1990, **64**, 31-40.
30. D. Chen, H. P. Rebo, A. Gronvold, K. Moljord and A. Holmen, *Microporous and Mesoporous Materials*, 2000, **35-36**, 121-135.
31. E. Aghaei and M. Haghighi, *Powder Technology*, 2015, **269**, 358-370.
32. S. Aghamohammadi and M. Haghighi, *Chemical Engineering Journal*, 2015, **264**, 359-375.
33. M. Kang, *Journal of Molecular Catalysis A: Chemical*, 2000, **160**, 437-444.
34. M. Hartmann and L. Kevan, *Research on Chemical Intermediates*, 2002, **28**, 625-695.
35. F. C. Sena, B. F. de Souza, N. C. de Almeida, J. S. Cardoso and L. D. Fernandes, *Applied Catalysis A: General*, 2011, **406**, 59-62.
36. J. Lu, X. Wang and H. Li, *Reaction Kinetics and Catalysis Letters*, 2009, **97**, 255-261.
37. X. Zhang, R. Wang, X. Yang and F. Zhang, *Microporous and Mesoporous Materials*, 2008, **116**, 210-215.

38. E. Aghaei and M. Haghghi, *Microporous and Mesoporous Materials*, 2014, **196**, 179-190.
39. J. M. Campelo, F. Lafont, J. M. Marinas and M. Ojeda, *Applied Catalysis A: General*, 2000, **192**, 85-96.
40. S. Seelan and A. K. Sinha, *Journal of Molecular Catalysis A: Chemical*, 2004, **215**, 149-152.
41. T. Álvaro-Muñoz, C. Márquez-Álvarez and E. Sastre, *Catalysis Today*, 2012, **179**, 27-34.
42. N. Nishiyama, M. Kawaguchi, Y. Hirota, D. Van Vu, Y. Egashira and K. Ueyama, *Applied Catalysis A: General*, 2009, **362**, 193-199.
43. Y. Wei, D. Zhang, L. Xu, F. Chang, Y. He, S. Meng, B.-l. Su and Z. Liu, *Catalysis Today*, 2008, **131**, 262-269.
44. M. D. Abramoff, P. J. Magalhaes and S. J. Ram, *Biophotonics International*, 2004, **11**, 36-42.
45. S. R. Venna and M. A. Carreon, *Journal of Materials Chemistry*, 2009, **19**, 3138-3140.
46. M. Salmasi, S. Fatemi and S. J. Hashemi, *Scientia Iranica*, 2012, **19**, 1632-1637.
47. M. Salmasi, S. Fatemi and A. Taheri Najafabadi, *Journal of Industrial and Engineering Chemistry*, 2011, **17**, 755-761.
48. G. Liu, P. Tian, J. Li, D. Zhang, F. Zhou and Z. Liu, *Microporous and Mesoporous Materials*, 2008, **111**, 143-149.
49. S. Aghamohammadi, M. Haghghi and S. Karimipour, *Journal of Nanoscience and Nanotechnology*, 2013, **13**, 4872-4882.
50. Y. Vafaeian, M. Haghghi and S. Aghamohammadi, *Energy Conversion and Management*, 2013, **76**, 1093-1103.
51. Z. Abbasi, M. Haghghi, E. Fatehifar and S. Saedy, *International Journal of Chemical Reactor Engineering*, 2011, **9**, 1-19.
52. R. Khoshbin and M. Haghghi, *Journal of Nanoscience and Nanotechnology*, 2013, **13**, 4996-5003.
53. S. M. Sajjadi, M. Haghghi and F. Rahmani, *Journal of Sol-Gel Science and Technology*, 2014, **70**, 111-124.
54. K. Hemelsoet, A. Ghysels, D. Mores, K. De Wispelaere, V. Van Speybroeck, B. M. Weckhuysen and M. Waroquier, *Catalysis Today*, 2011, **177**, 12-24.

55. Y. Wei, D. Zhang, Y. He, L. Xu, Y. Yang, B.-L. Su and Z. Liu, *Catalysis Letters*, 2007, **114**, 30-35.
56. S. M. Sajjadi, M. Haghghi, A. Alizadeh Eslami and F. Rahmani, *Journal of Sol-Gel Science and Technology*, 2013, **67**, 601-617.
57. S. Saedy, M. Haghghi and M. Amirkhosrow, *Particuology*, 2012, **10**, 729-736.

Figure Captions

- Figure 1. Preparation steps of nanostructured LaAPSO-34 catalyst with different Si/Al ratios. 26
- Figure 2. Experimental setup for activity test of nanostructured LaAPSO-34 catalyst used in conversion of methanol to light olefins. 27
- Figure 3. XRD patterns of nanostructured LaAPSO-34 catalyst synthesized with different Si/Al ratios: (a) LaAPSO-34 (0.1), (b) LaAPSO-34 (0.2), (c) SAPO-34 (0.3), (d) LaAPSO-34 (0.3) and (e) LaAPSO-34 (0.4). 28
- Figure 4. Crystallite size and relative crystallinity of nanostructured LaAPSO-34 catalyst synthesized with different Si/Al ratios. 29
- Figure 5. FESEM images of nanostructured LaAPSO-34 catalyst synthesized with different Si/Al ratios: (a) LaAPSO-34 (0.1), (b) LaAPSO-34 (0.2), (c) SAPO-34 (0.3), (d) LaAPSO-34 (0.3) and (e) LaAPSO-34 (0.4). 30
- Figure 6. Particle size histogram of La-doped SAPO-34 catalyst: (a) SAPO-34 (0.3) and (b) LaAPSO-34 (0.3). 31
- Figure 7. EDX dot-mapping analysis of nanostructured LaAPSO-34 catalyst synthesized with different Si/Al ratios: (a) LaAPSO-34 (0.1), (b) LaAPSO-34 (0.2), (c) LaAPSO-34 (0.3) and (d) LaAPSO-34 (0.4). 32
- Figure 8. Gel vs. crystal composition of nanostructured LaAPSO-34 catalyst synthesized with different Si/Al ratios: (a) LaAPSO-34 (0.1), (b) LaAPSO-34 (0.2), (c) LaAPSO-34 (0.3) and (d) LaAPSO-34 (0.4). 33
- Figure 9. TEM images of nanostructured LaAPSO-34 catalyst: LaAPSO-34 (0.3). 34
- Figure 10. BET surface area analysis of nanostructured LaAPSO-34 catalyst synthesized with different Si/Al ratios. 34
- Figure 11. FTIR spectra of nanostructured LaAPSO-34 catalyst synthesized with different Si/Al ratios: (a) LaAPSO-34 (0.1), (b) LaAPSO-34 (0.2), (c) SAPO-34 (0.3), (d) LaAPSO-34 (0.3) and (e) LaAPSO-34 (0.4). 35
- Figure 12. TPD-NH₃ analysis of nanostructured La-doped SAPO-34 catalysts synthesized at different crystallization time: (a) LaAPSO-34 (0.2), (b) SAPO-34 (0.3) and (c) LaAPSO-34 (0.3). 36
- Figure 13. Effect of temperature on (a) methanol conversion and (b) products selectivities over LaAPSO-34 (0.1), GHSV=4200 cm³/g_{cat}.h, temperature=300-500 °C, feed: 30% methanol, 1 g catalyst. 37
- Figure 14. Effect of La addition on methanol conversion: (SAPO-34 (0.3) vs. LaAPSO-34 (0.3)), GHSV=4200 cm³/g_{cat}.h, temperature=300-500 °C, feed: 30% methanol, 1 g catalyst. 38

- Figure 15. Effect of La addition on olefins selectivities (SAPO-34 (0.3) vs. LaAPSO-34 (0.3)): (a) C₂H₄ and (b) C₃H₆, GHSV=4200 cm³/g_{cat}-h, temperature=300-500 °C, feed: 30% methanol, 1 g catalyst. 39
- Figure 16. Effect of La addition on methane selectivity (SAPO-34 (0.3) vs. LaAPSO-34 (0.3)), 40
- Figure 17. Effect of Si/Al ratio on methanol conversion and products selectivity over nanostructured LaAPSO-34: (a) LaAPSO-34 (0.1), (b) LaAPSO-34 (0.2), (c) SAPO-34 (0.3), (d) LaAPSO-34 (0.3) and (e) LaAPSO-34 (0.4), GHSV=4200 cm³/g_{cat}-h, temperature=350 °C, feed: 30% methanol, 1 g catalyst. 41

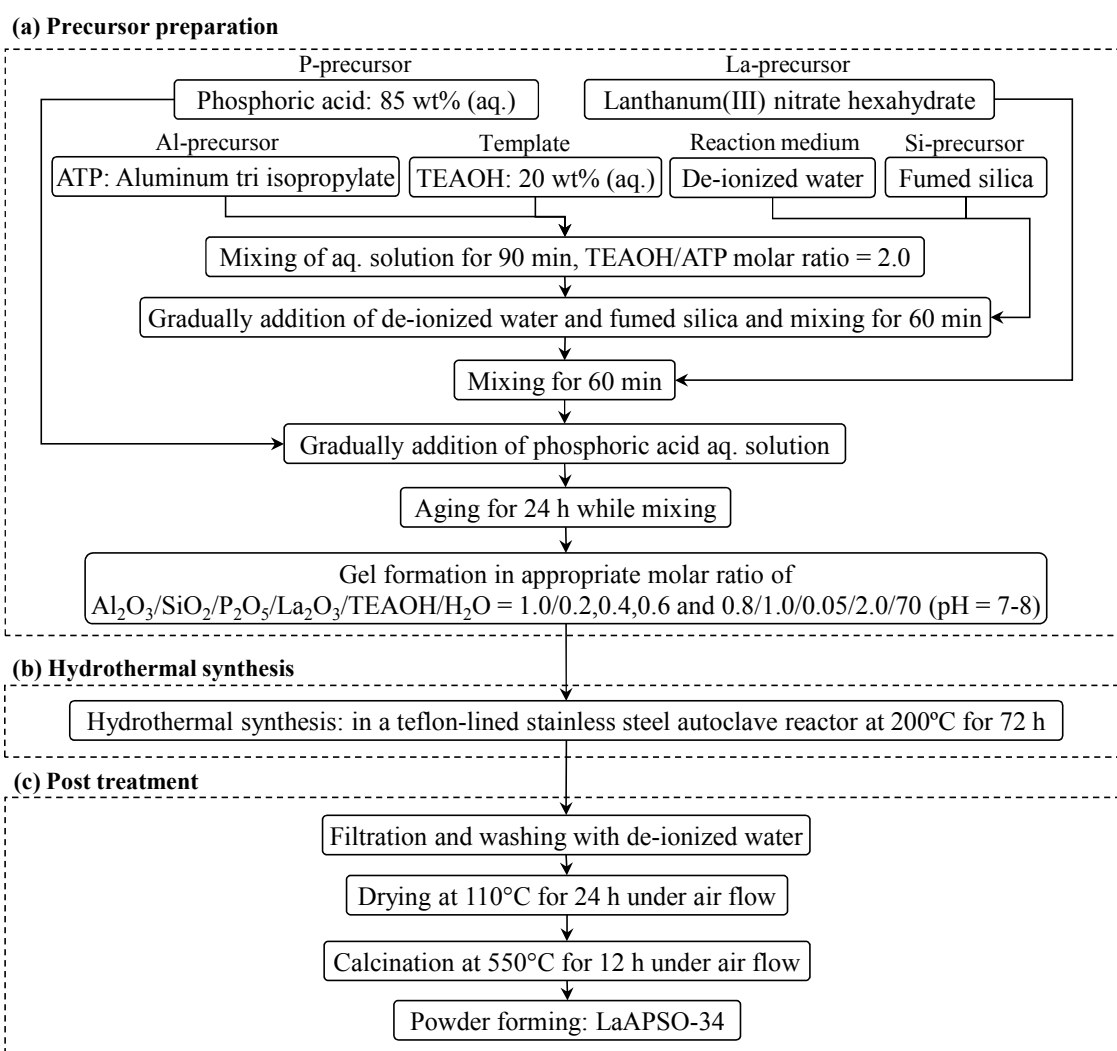
Tables Caption

- Table 1. Unit cell parameters and unit cell volume of samples. 26

Figures and Tables

Table 1. Unit cell parameters and unit cell volume of samples.

Catalyst	a = b (Å)	c (Å)	V (Å ³)
LaAPSO-34 (0.1)	13.69	14.53	2356.21
LaAPSO-34 (0.2)	13.60	15.10	2420.77
SAPO-34 (0.3)	13.62	14.71	2364.87
LaAPSO-34 (0.3)	13.64	14.76	2376.88
LaAPSO-34 (0.4)	13.56	14.62	2329.03

**Figure 1. Preparation steps of nanostructured LaAPSO-34 catalyst with different Si/Al ratios.**

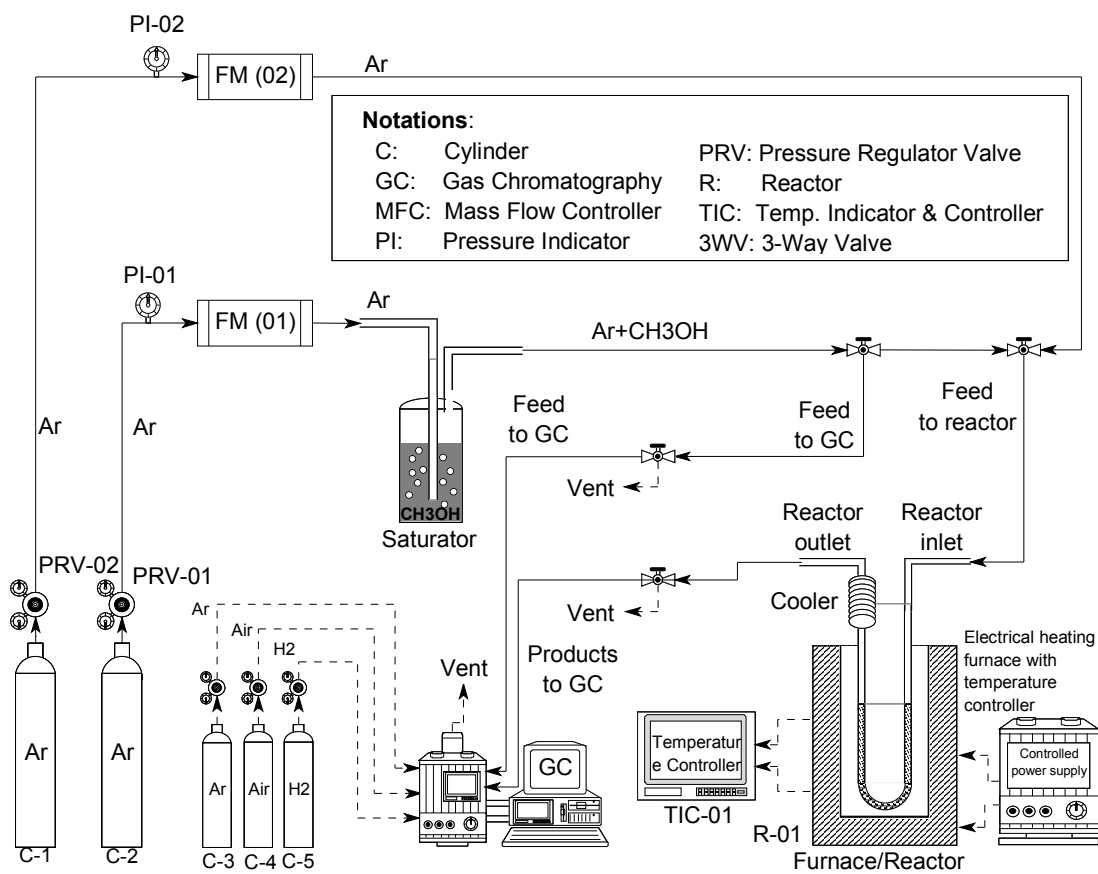


Figure 2. Experimental setup for activity test of nanostructured LaAPSO-34 catalyst used in conversion of methanol to light olefins.

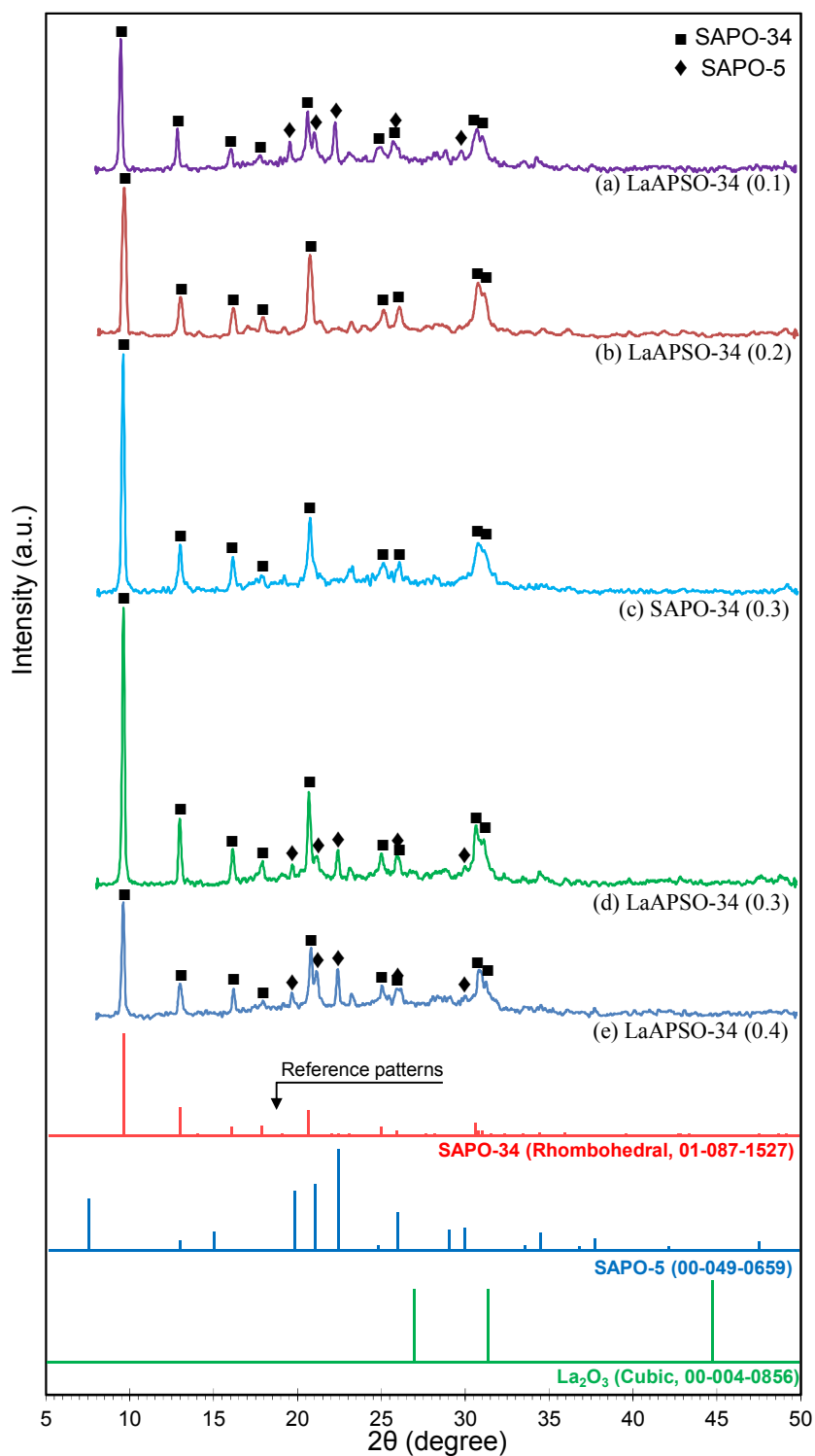


Figure 3. XRD patterns of nanostructured LaAPSO-34 catalyst synthesized with different Si/Al ratios: (a) LaAPSO-34 (0.1), (b) LaAPSO-34 (0.2), (c) SAPO-34 (0.3), (d) LaAPSO-34 (0.3) and (e) LaAPSO-34 (0.4).

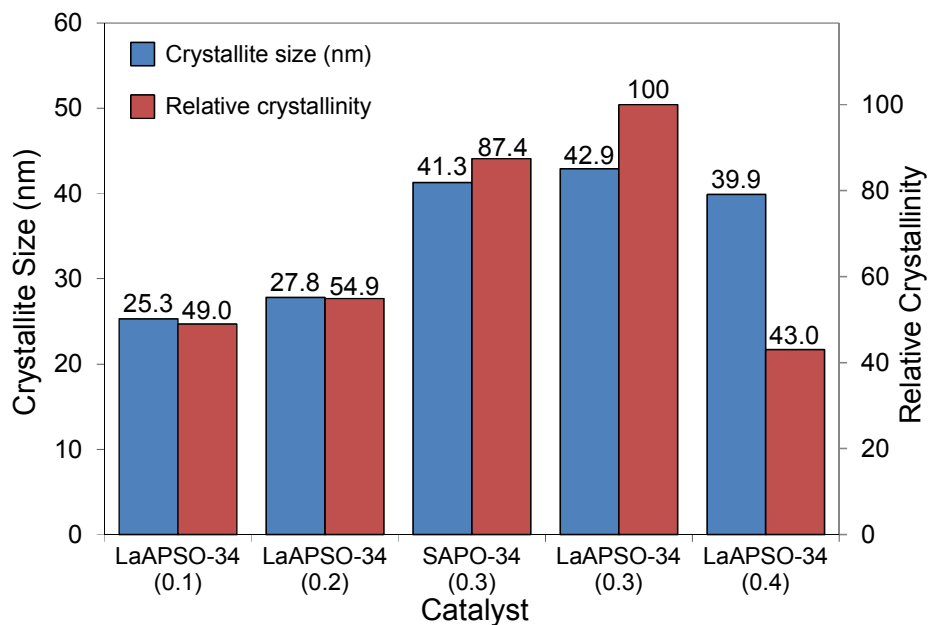


Figure 4. Crystallite size and relative crystallinity of nanostructured LaAPSO-34 catalyst synthesized with different Si/Al ratios.

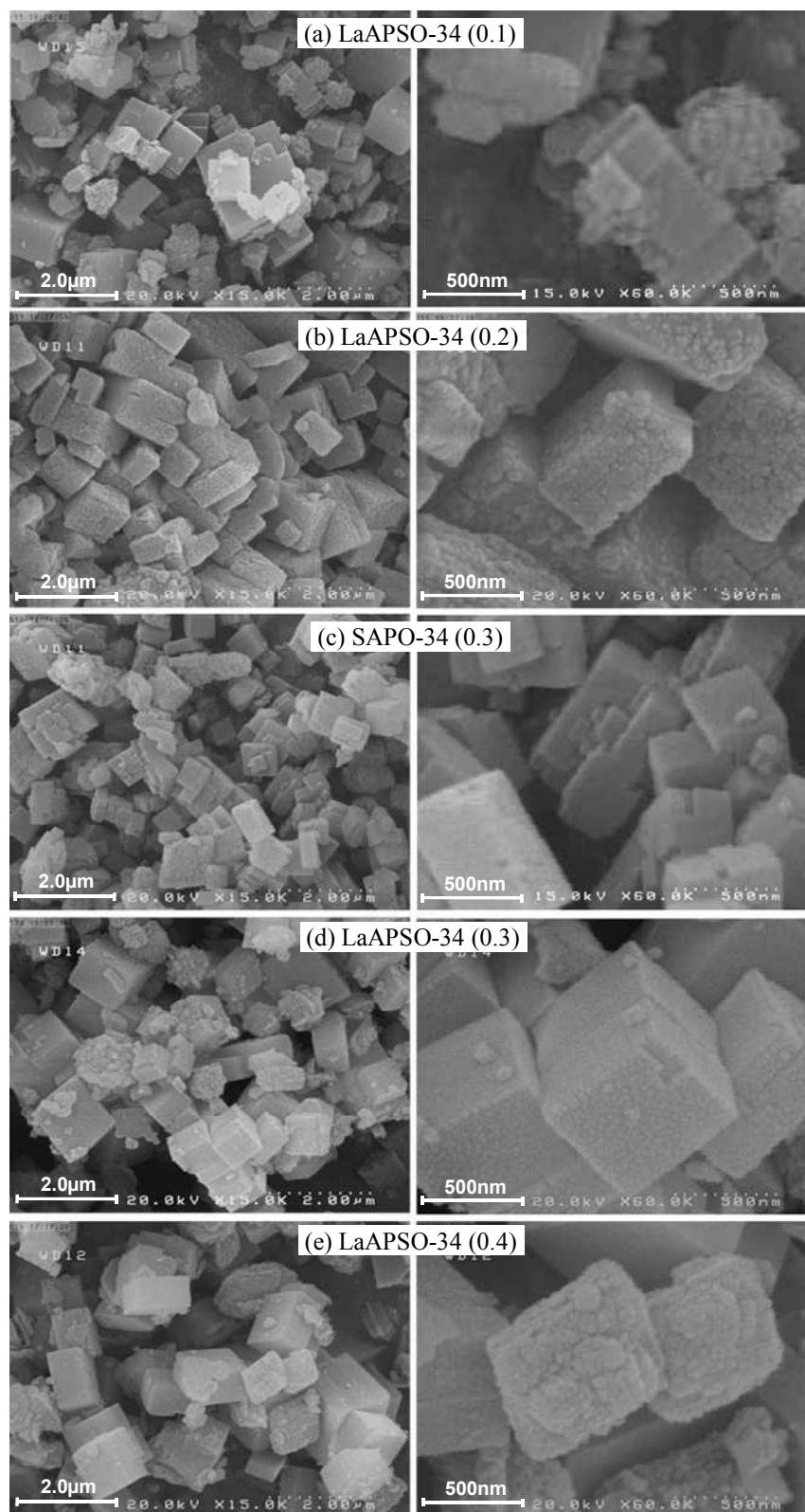


Figure 5. FESEM images of nanostructured LaAPSO-34 catalyst synthesized with different Si/Al ratios: (a) LaAPSO-34 (0.1), (b) LaAPSO-34 (0.2), (c) SAPO-34 (0.3), (d) LaAPSO-34 (0.3) and (e) LaAPSO-34 (0.4).

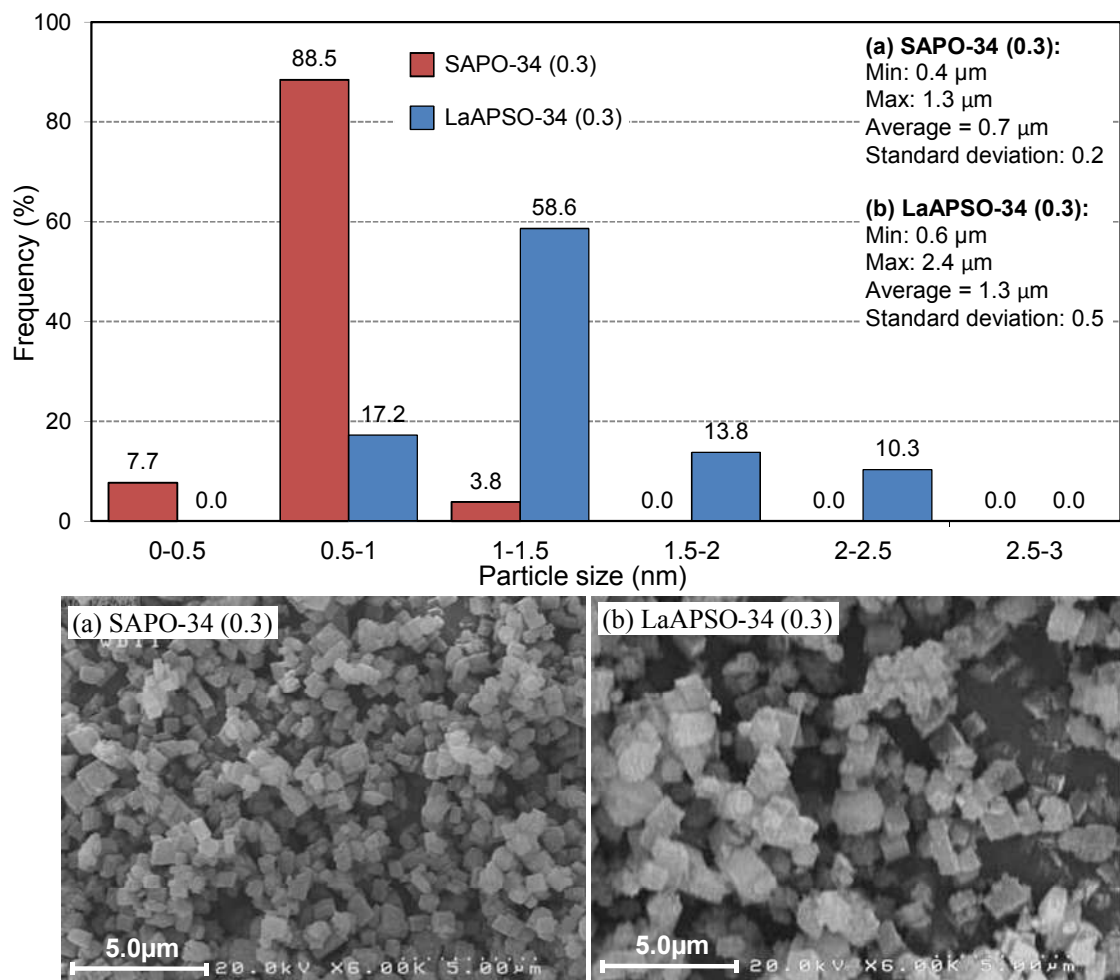


Figure 6. Particle size histogram of La-doped SAPO-34 catalyst: (a) SAPO-34 (0.3) and (b) LaAPSO-34 (0.3).

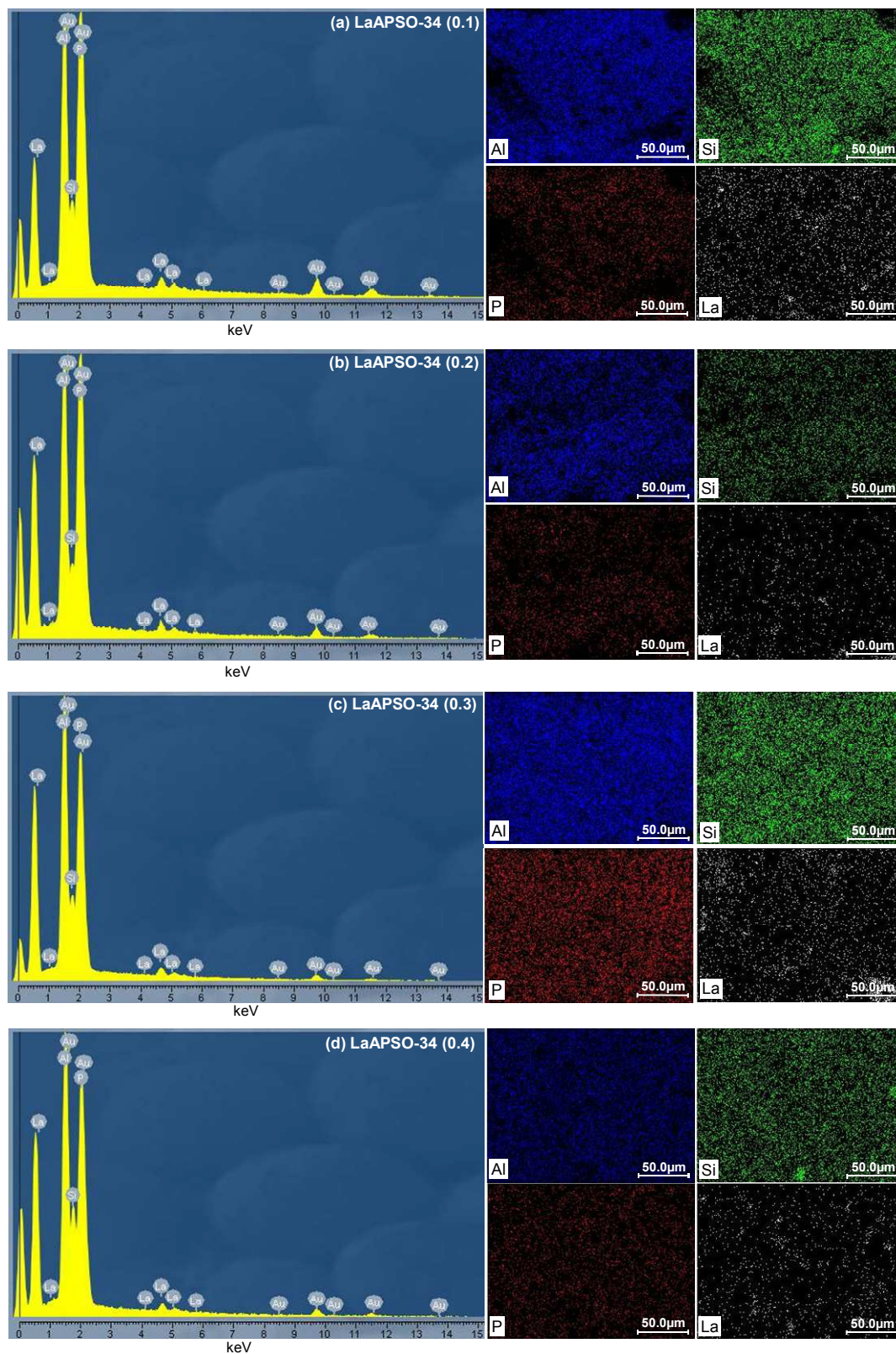


Figure 7. EDX dot-mapping analysis of nanostructured LaAPSO-34 catalyst synthesized with different Si/Al ratios: (a) LaAPSO-34 (0.1), (b) LaAPSO-34 (0.2), (c) LaAPSO-34 (0.3) and (d) LaAPSO-34 (0.4).

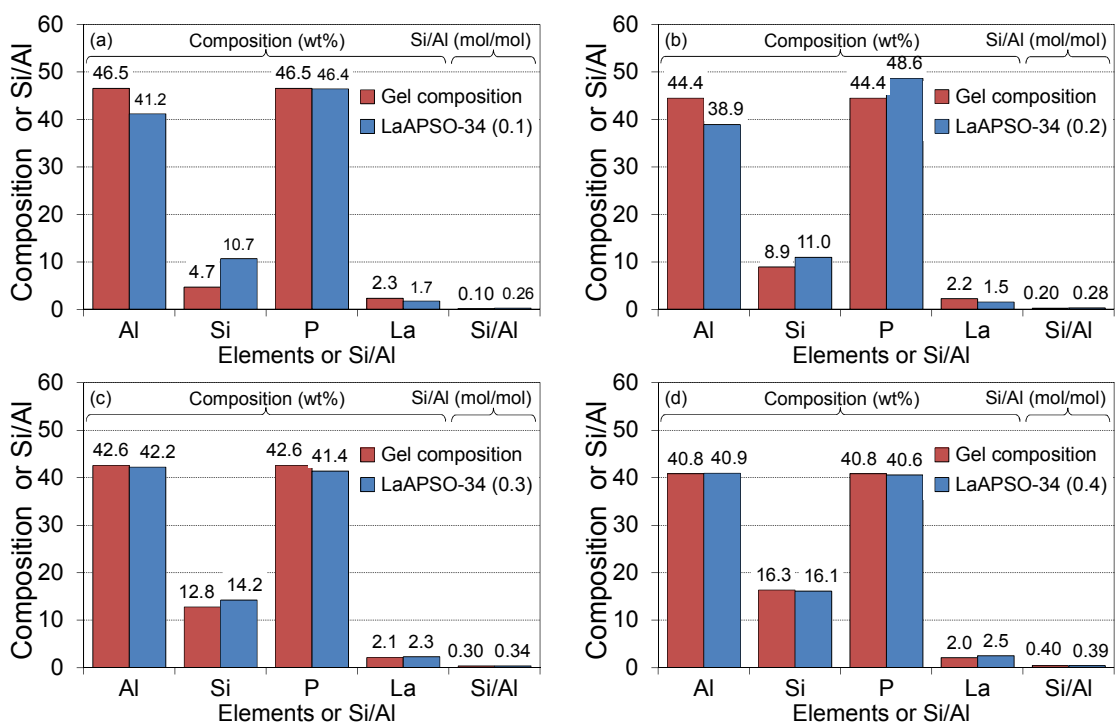


Figure 8. Gel vs. crystal composition of nanostructured LaAPSO-34 catalyst synthesized with different Si/Al ratios: (a) LaAPSO-34 (0.1), (b) LaAPSO-34 (0.2), (c) LaAPSO-34 (0.3) and (d) LaAPSO-34 (0.4).

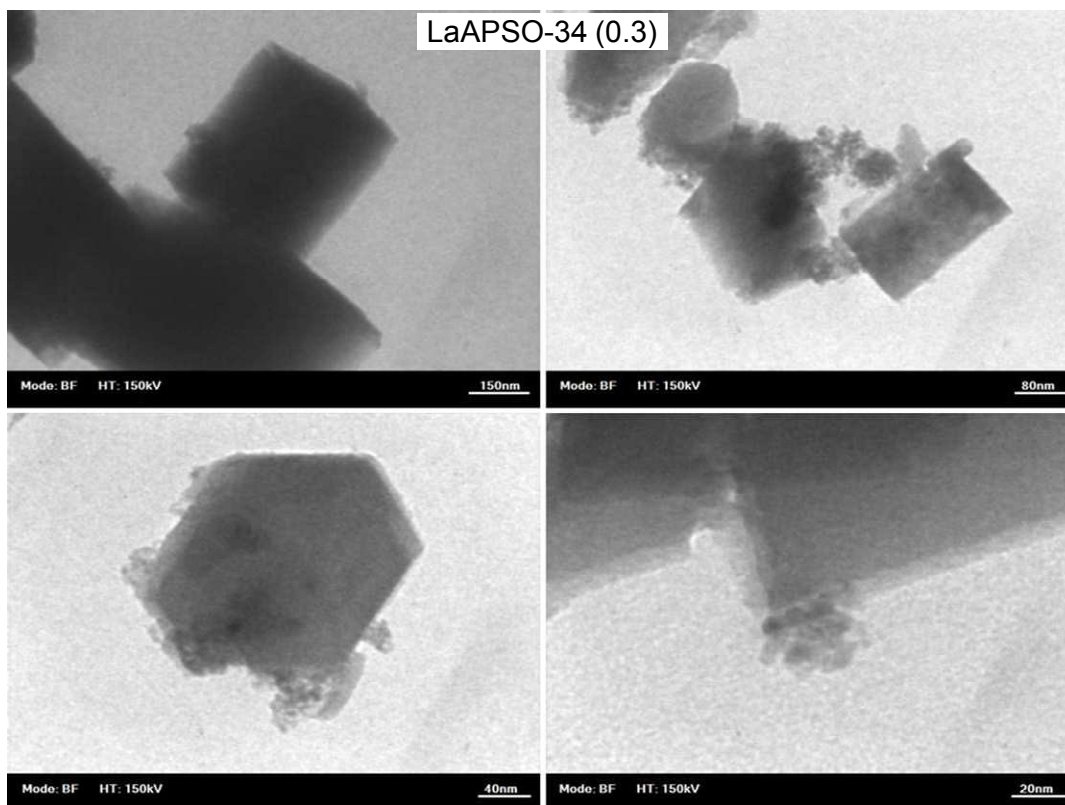


Figure 9. TEM images of nanostructured LaAPSO-34 catalyst: LaAPSO-34 (0.3).

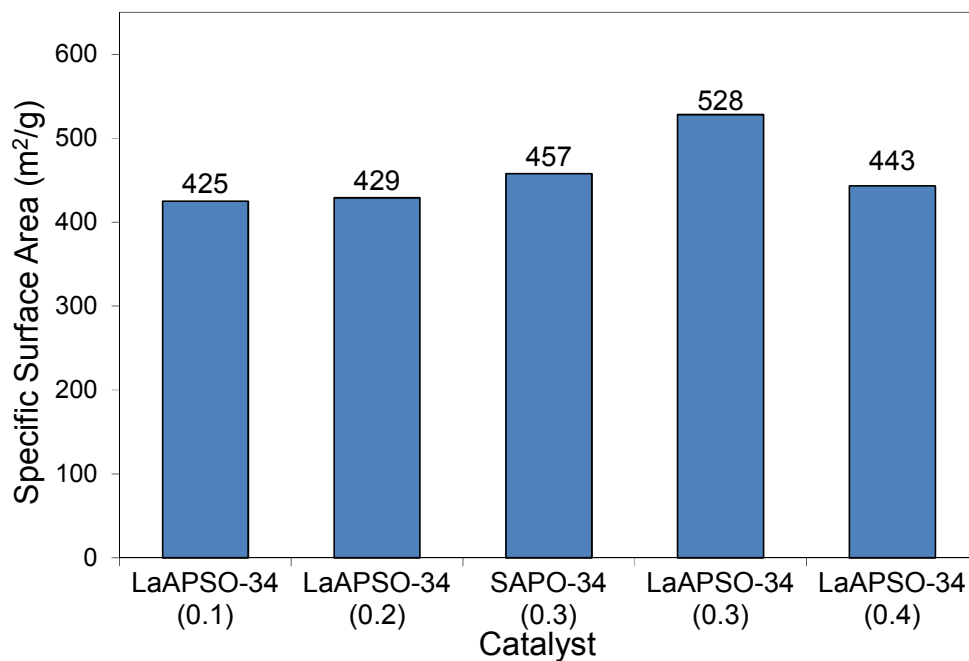


Figure 10. BET surface area analysis of nanostructured LaAPSO-34 catalyst synthesized with different Si/Al ratios.

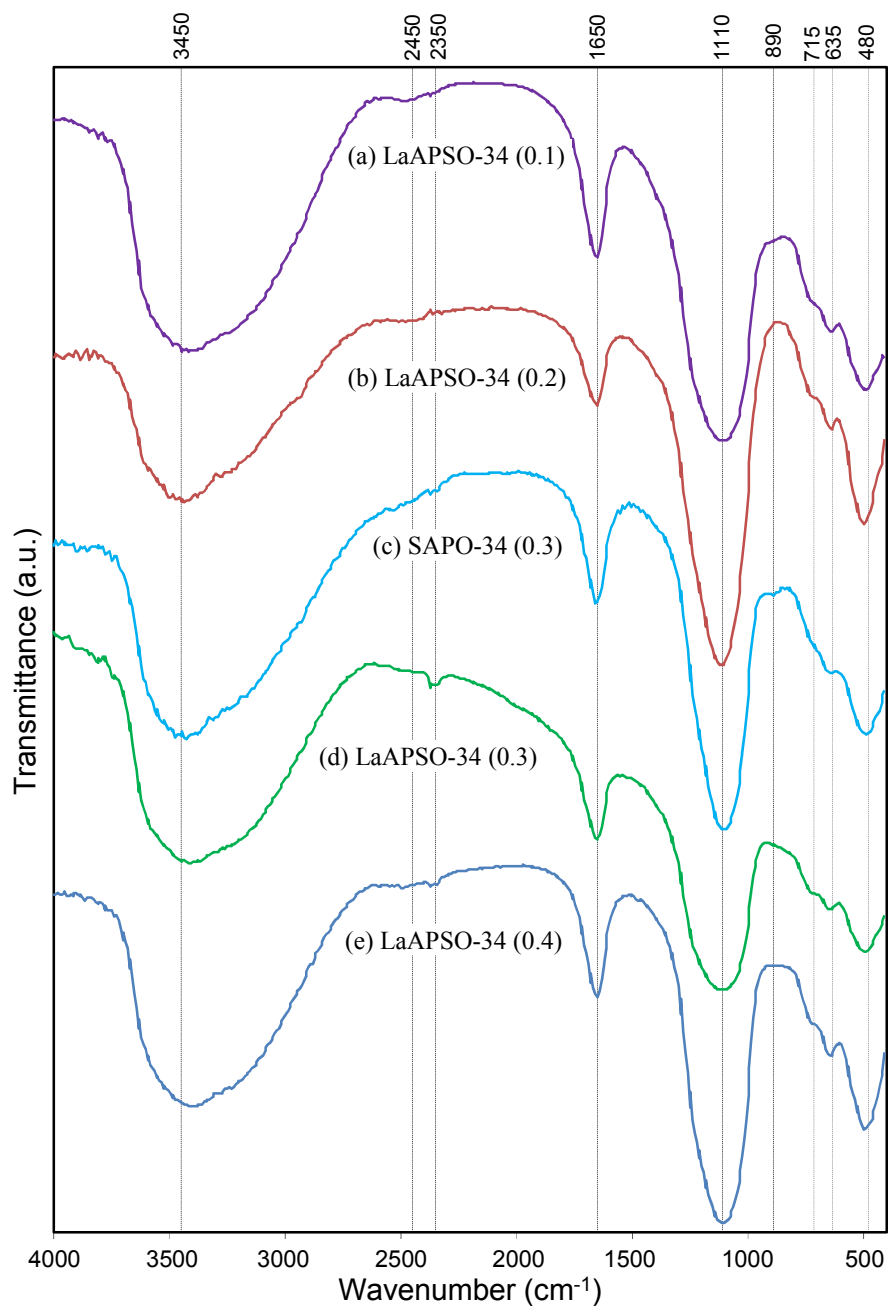


Figure 11. FTIR spectra of nanostructured LaAPSO-34 catalyst synthesized with different Si/Al ratios: (a) LaAPSO-34 (0.1), (b) LaAPSO-34 (0.2), (c) SAPO-34 (0.3), (d) LaAPSO-34 (0.3) and (e) LaAPSO-34 (0.4).

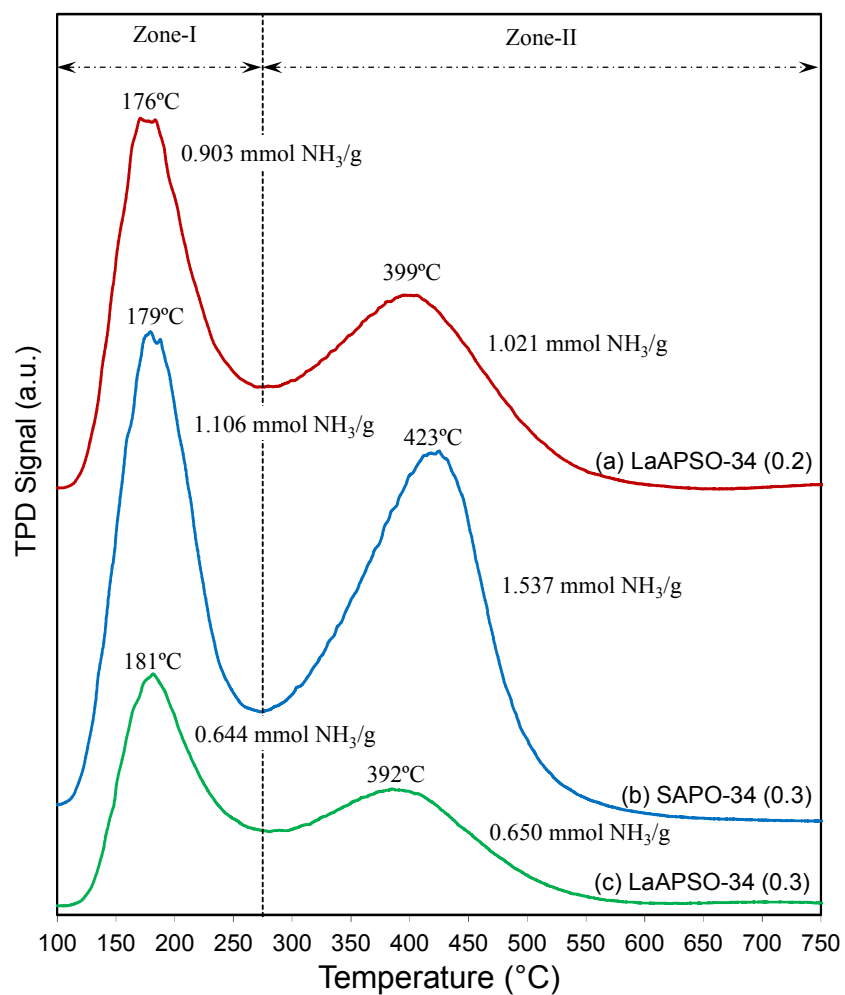


Figure 12. TPD-NH₃ analysis of nanostructured La-doped SAPO-34 catalysts synthesized at different crystallization time: (a) LaAPSO-34 (0.2), (b) SAPO-34 (0.3) and (c) LaAPSO-34 (0.3).

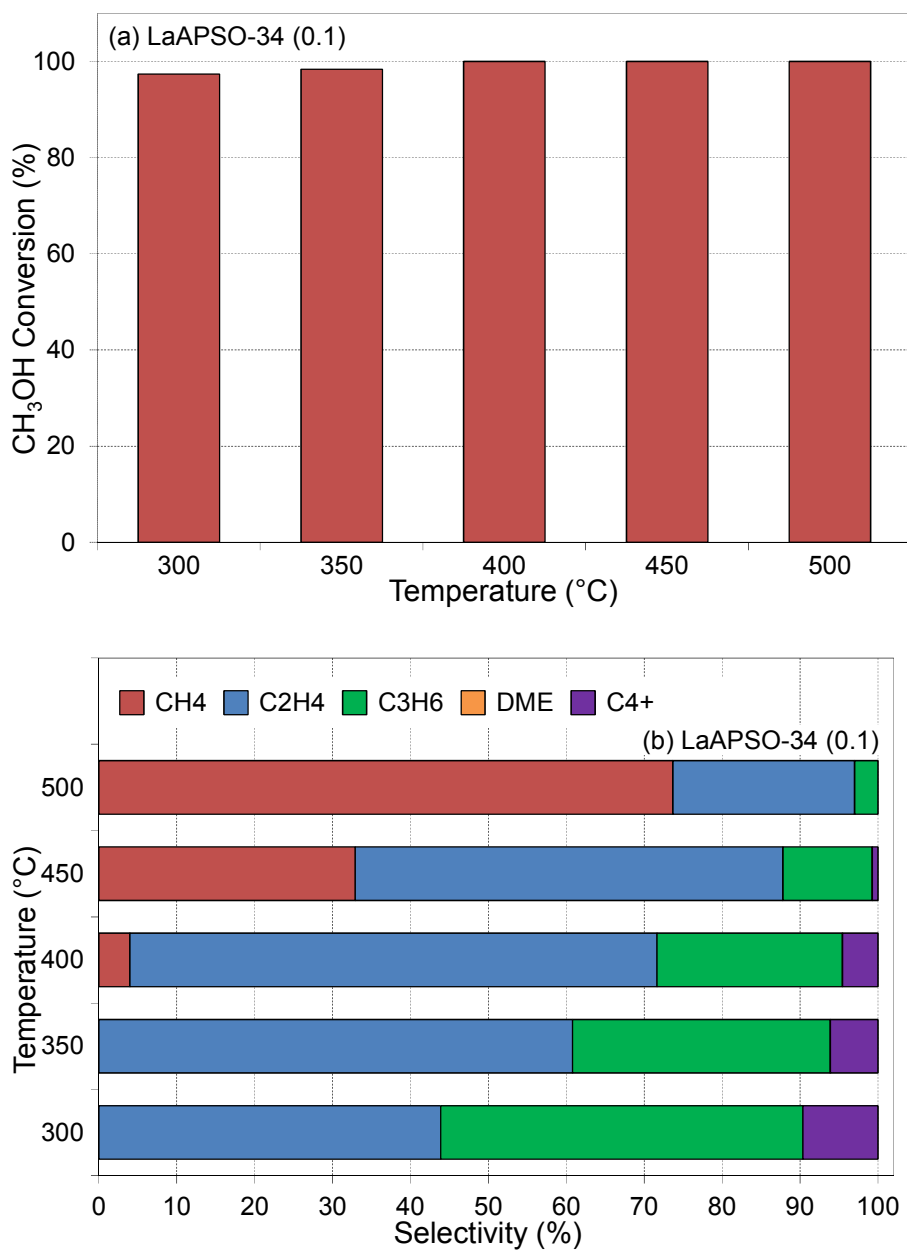


Figure 13. Effect of temperature on (a) methanol conversion and (b) products selectivities over LaAPSO-34 (0.1), GHSV=4200 cm³/g_{cat}.h, temperature=300-500 °C, feed: 30% methanol, 1 g catalyst.

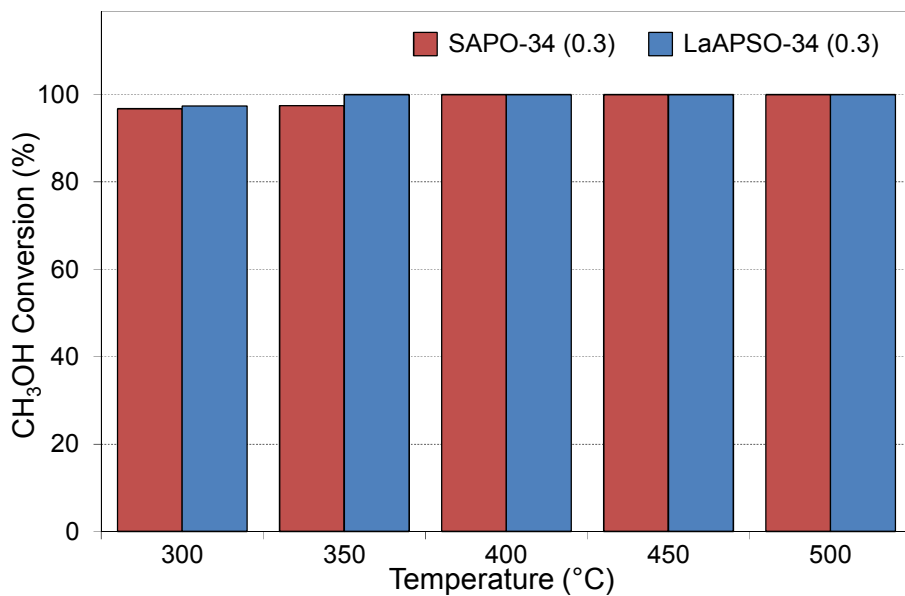


Figure 14. Effect of La addition on methanol conversion: (SAPO-34 (0.3) vs. LaAPSO-34 (0.3)), GHSV=4200 cm³/g_{cat}.h, temperature=300-500 °C, feed: 30% methanol, 1 g catalyst.

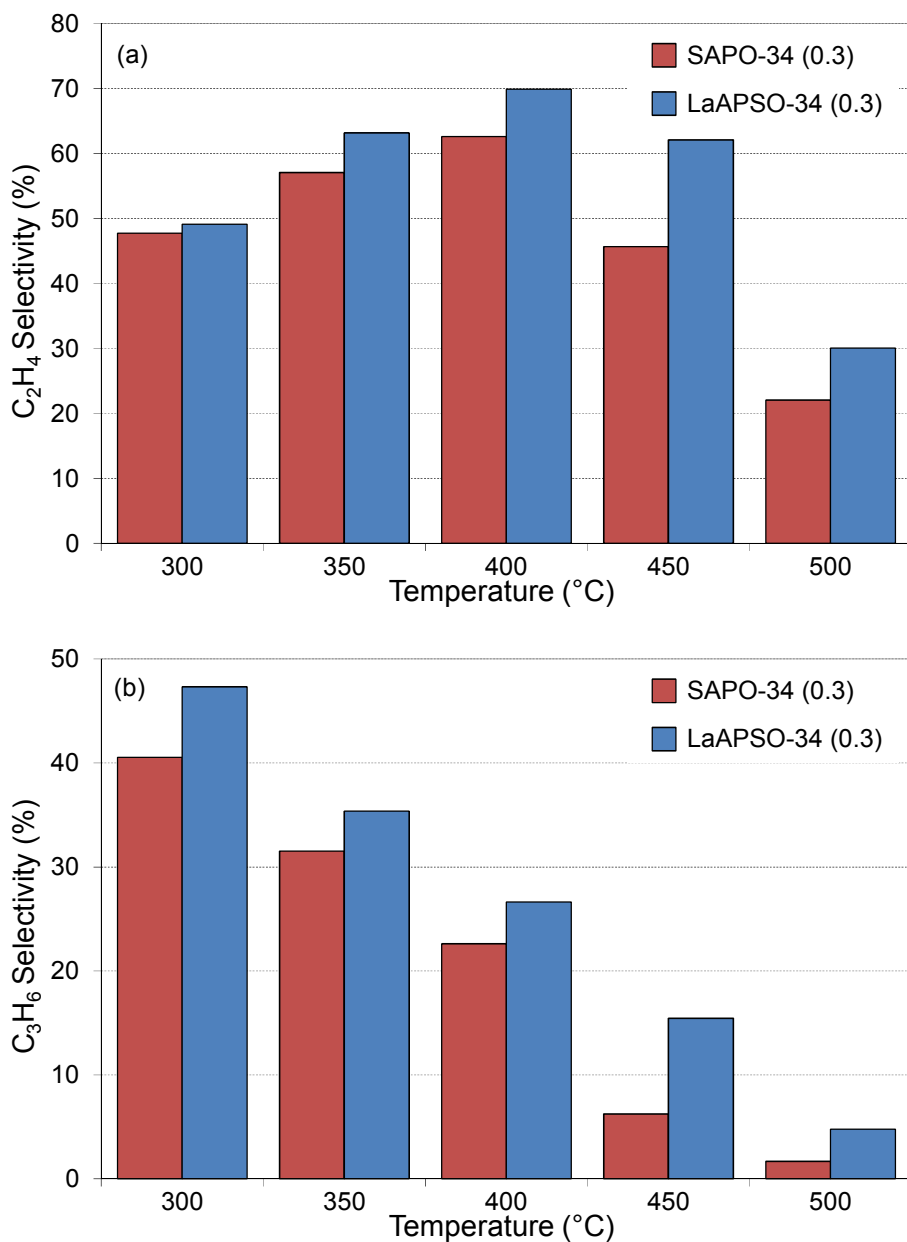


Figure 15. Effect of La addition on olefins selectivities (SAPO-34 (0.3) vs. LaAPSO-34 (0.3)): (a) C₂H₄ and (b) C₃H₆, GHSV=4200 cm³/g_{cat}·h, temperature=300-500 °C, feed: 30% methanol, 1 g catalyst.

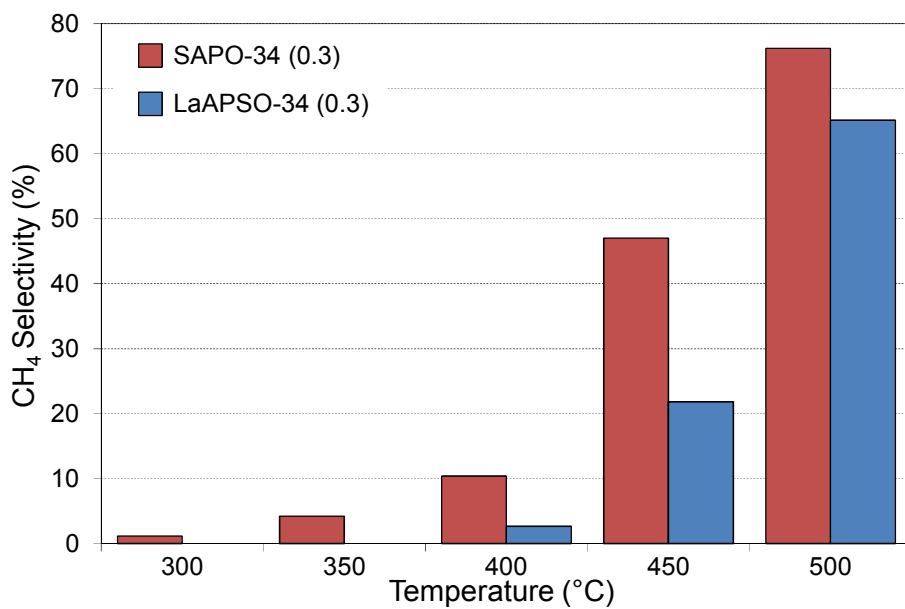


Figure 16. Effect of La addition on methane selectivity (SAPO-34 (0.3) vs. LaAPSO-34 (0.3)), GHSV=4200 cm³/g_{cat}.h, temperature=300-500 °C, feed: 30% methanol, 1 g catalyst.

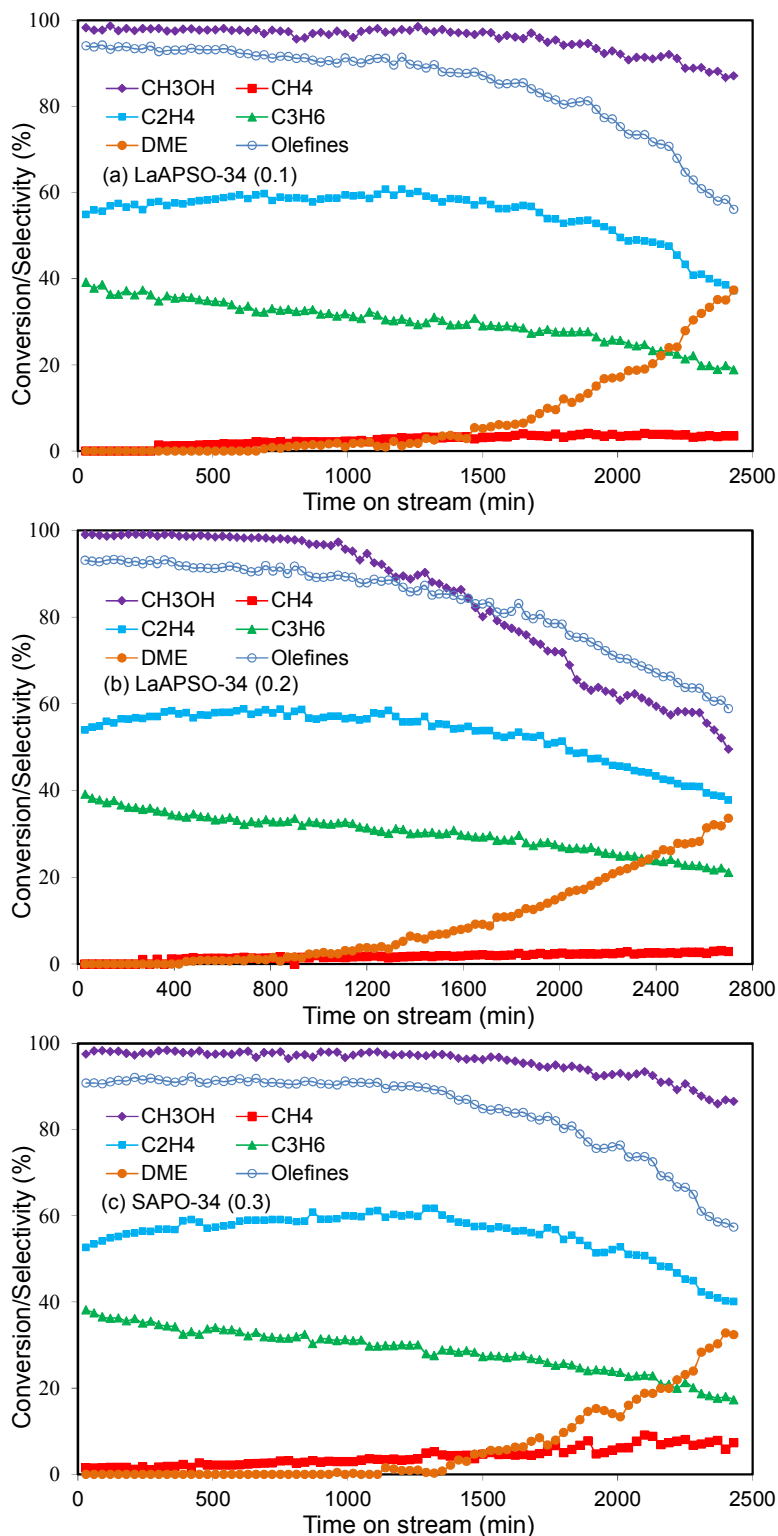


Figure 17. Effect of Si/Al ratio on methanol conversion and products selectivity over nanostructured LaAPSO-34: (a) LaAPSO-34 (0.1), (b) LaAPSO-34 (0.2), (c) SAPO-34 (0.3), (d) LaAPSO-34 (0.3) and (e) LaAPSO-34 (0.4), GHSV=4200 cm³/g_{cat}·h, temperature=350 °C, feed: 30% methanol, 1 g catalyst.

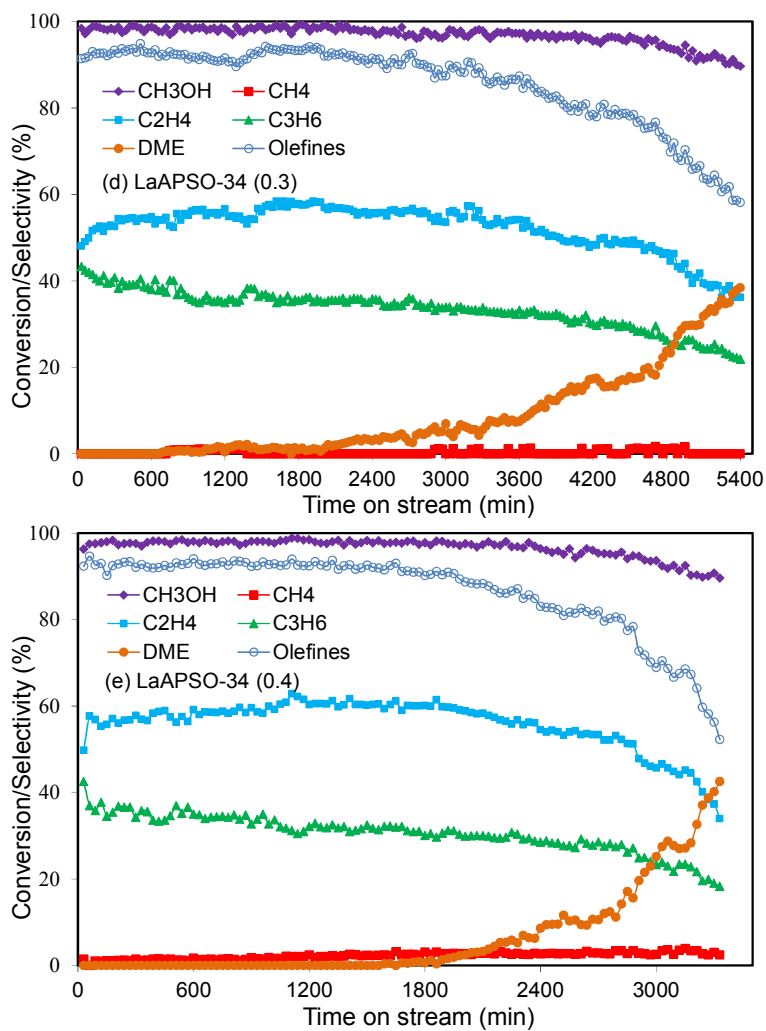


Figure 17. Continued.

Enhancement of Catalytic Properties and Lifetime of Nanostructured SAPO-34 by La Isomorphous Substitution and Alteration of Si/Al Ratio Used in Methanol to Light Olefins

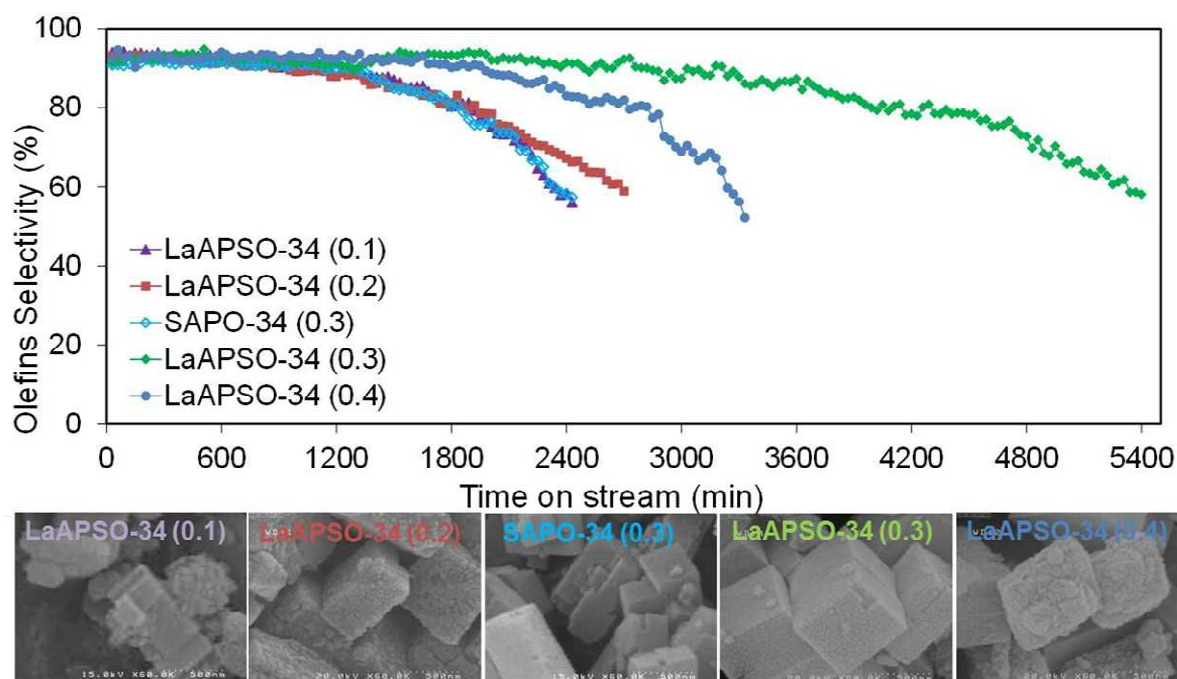
Abolfazl Amoozegar^{1,2}, Mohammad Haghighi^{*1,2}, Sogand Aghamohammadi^{1,2}

1. Chemical Engineering Faculty, Sahand University of Technology, P.O.Box 51335-1996, Sahand New Town, Tabriz, Iran.

2. Reactor and Catalysis Research Center (RCRC), Sahand University of Technology, P.O.Box 51335-1996, Sahand New Town, Tabriz, Iran.

Graphical Abstract

Methanol conversion to light olefins was investigated over SAPO-34 catalysts with La introduction exploring the effect of different Si/Al ratios. The catalysts were prepared via hydrothermal method and characterized with XRD, FESEM, EDX, TEM, BET and FTIR techniques. La incorporation in to the crystalline framework would diminish the effect of side reactions. The outstanding catalytic lifetime of the La modified catalyst with optimum Si content was reported to be 5500 min sustaining light olefins selectivity at higher values at diminished reaction temperature of 350 °C.



* Corresponding author:

Reactor and Catalysis Research Center, Sahand University of Technology, P.O. Box 51335-1996, Sahand New Town, Tabriz, Iran. Email: haghighi@sut.ac.ir, Tel: +98-41-33458096 & +98-41-33459152, Fax: +98-41-33444355, web: <http://rcrc.sut.ac.ir>